Journal of Quantitative Spectroscopy & Radiative Transfer 192 (2017) 14–29

Contents lists available at ScienceDirect

Journal of Quantitative Spectroscopy & Radiative Transfer

journal homepage: www.elsevier.com/locate/jqsrt

An algorithm for hyperspectral remote sensing of aerosols: 2. Information content analysis for aerosol parameters and principal components of surface spectra

Weizhen Hou [a], Jun Wang [a,b,*], Xiaoguang Xu [a,b], Jeffrey S. Reid [c]

[a] Department of Earth and Atmospheric Sciences, University of Nebraska–Lincoln, 303, Lincoln, NE 68588, USA
[b] Now at Department of Chemical and Biochemical Engineering, Center of Global and Regional Environmental Research, The University of Iowa, 4133 Seamans Center, Iowa City, IA 52242, USA
[c] Marine Meteorology Division, Naval Research Laboratory, 7 Grace Hopper Ave, Stop 2, Monterey, CA 93943, USA

ARTICLE INFO

Article history:
Received 7 October 2016
Received in revised form
1 January 2017
Accepted 3 January 2017
Available online 4 February 2017

Keywords:
TEMPO
Geostationary satellite
Information content analysis
Degrees of freedom for signal
Principal component
Hyperspectral remote sensing
Common band selection

ABSTRACT

This paper describes the second part of a series of investigation to develop algorithms for simultaneous retrieval of aerosol parameters and surface reflectance from the future hyperspectral and geostationary satellite sensors such as Tropospheric Emissions: Monitoring of POllution (TEMPO). The information content in these hyperspectral measurements is analyzed for 6 principal components (PCs) of surface spectra and a total of 14 aerosol parameters that describe the columnar aerosol volume V_{total}, fine-mode aerosol volume fraction, and the size distribution and wavelength-dependent index of refraction in both coarse and fine mode aerosols. Forward simulations of atmospheric radiative transfer are conducted for 5 surface types (green vegetation, bare soil, rangeland, concrete and mixed surface case) and a wide range of aerosol mixtures. It is shown that the PCs of surface spectra in the atmospheric window channel could be derived from the top-of-the-atmosphere reflectance in the conditions of low aerosol optical depth (AOD $\leq$ 0.2 at 550 nm), with a relative error of 1%. With degree freedom for signal analysis and the sequential forward selection method, the common bands for different aerosol mixture types and surface types can be selected for aerosol retrieval. The first 20% of our selected bands accounts for more than 90% of information content for aerosols, and only 4 PCs are needed to reconstruct surface reflectance. However, the information content in these common bands from each TEMPO individual observation is insufficient for the simultaneous retrieval of surface's PC weight coefficients and multiple aerosol parameters (other than V_{total}). In contrast, with multiple observations for the same location from TEMPO in multiple consecutive days, 1–3 additional aerosol parameters could be retrieved. Consequently, a self-adjustable aerosol retrieval algorithm to account for surface types, AOD conditions, and multiple-consecutive observations is recommended to derive aerosol parameters and surface reflectance simultaneously from TEMPO.

1. Introduction

Atmospheric aerosol properties, especially aerosol optical depth (AOD), have been retrieved routinely from satellite remote sensing since 1990s [1]. While various algorithms have been developed, one of the common and most challenging component in these algorithms is the decoupling of the surface and atmospheric contributions (or path radiance) from the satellite-observed reflectance spectra at the top of atmosphere (TOA), after which aerosol properties can be derived from the path radiance with the correction of Rayleigh scattering and gas absorption [2]. This decoupling is often more complicated over the land than over the ocean for the reason that the contribution of land surface to the radiance measured at the top-of-atmosphere (TOA) is much larger and has various spatial variability in general [3]. Consequently, as shown in Table 1 (for expansion of different satellite acronyms), past algorithms have avoided to conduct retrievals at the spectrum where surface reflectance are high, and instead, focused on the retrieval from use of the spectrum with low land surface reflectance, such as the MODIS visible bands over the vegetated dark target (DT) surfaces [4,5], the MODIS and SeaWiFS "deep blue"

* Corresponding author at: Department of Chemical and Biochemical Engineering, Center for Global and Regional Environmental Research, The University of Iowa, 4133 Seamans Center, Iowa City, IA 52242, USA.
E-mail address: jun-wang-1@uiowa.edu (J. Wang).

http://dx.doi.org/10.1016/j.jqsrt.2017.01.041
0022-4073/

Table 1
Aerosol parameters have been retrieved from satellite remote sensing.[a]

Senor	Full name	Parameters retrieved	Assumptions	Spectral used	References
MERIS	Medium Resolution Imaging Spectrometer	α	ρ^s estimated by linear mixing of different basic spectra with NDVI	412, 443, 665, 865 nm	[11,12]
SCIAMACHY	Scanning Imaging Absorption spectrometer for Atmospheric Chartography	AT	Global ρ^s derived from GOME observation	364, 387, 429, 683 nm	[10]
OMI	Ozone Monitoring Instrument	AT, ω, H, PSD	ρ^s from MISR	15 bands for 330 to 500 nm	[8,9]
		τ_a^{388nm}, ω^{388nm}	ρ^s from TOMS, dust height from GOCART	354, 388 nm	[9]
SeaWiFS	Sea-Viewing Wide Field-of-View Sensor	α	Global ρ^s dataset, BRDF	412, 490, 670 nm	[7]
MODIS	Moderate Resolution Imaging Spectroradiometer	α	Global ρ^s dataset, BRDF	412, 470, 650 nm	[6,7]
		α, η	The empirical relationship of ρ^s at 0.47 (0.66) μm with 2.12μm	0.47, 0.55, 0.66, 0.86, 1.24, 1.64, 2.12 μm	[4,5]
SEVIRI	Spinning Enhanced Visible and Infrared Imager	r_{eff}, AT, S^{550nm}	MODIS BRDF as a priori	0.64, 0.81, 1.64 μm	[17]
AATSR	Advance Along Track Scanning Radiometer	r_{eff}, AT	MODIS BRDF as a priori	0.55, 0.67, 0.87, 1.6μm, 2 views	[17]
MISR	Multi-angle Imaging SpectroRadiometer	AT, MC, SP	BRDF model	446, 558, 672, 866 nm, 9 views	[13–16]
POLDER	Polarization and Directionality of the Earth's Reflectance	α	Log-normal PSD (fine), a priori surface BRDF	490, 670, 865 nm, up to 16 views and polarization	[19–21]
AIRS	Atmospheric Infrared Sounder	$\tau_a^{10\mu m}$	r_{eff}, Height	8–12 μm	[22–24]

[a] The following symbols and acronyms are used in the table as follows. τ_a: AOD, ρ^s: surface reflectance, η: fine mode weighting, α: Ångström exponent, ω: single scatter albedo (SSA), r_{eff}: effective radius, H: height, S: bi-hemispherical albedo, PSD: particle size distribution, AT: aerosol type, MC: mixture of components, SP: (non-) spherical particles.

bands over the urban and semi-arid regions [6,7], and the OMI and SCIAMACHY's ultraviolet (UV) spectrum over ice-free and snow-free land surfaces [8–10]. Besides, some algorithms estimated the surface reflectance by linear mixing of different basic spectra of green vegetation and bare soil with the normalized different vegetation index (NDVI), such as Bremen Aerosol Retrieval (BAER) for MERIS [11,12]. Furthermore, measurements of polarization and/or from multi-angles are shown to make the derivation of path radiance relatively easier, even over the spectrum where surface reflectance is higher. Examples include the empirical orthogonal functions (EOF) algorithm for MISR [13–16], dual-view retrieval algorithm for AATSR [17,18], and polarized retrieval algorithm for POLDER [19–21]. In addition, the thermal infrared (TIR) atmospheric window in 8-12 μm also can be used for characterizing large aerosol particles (such as dust), such as the AIRS's algorithm [22–24]. Table 1 lists the major algorithms for remote sensing of aerosols, including their respective bands, assumptions for deriving surface reflectance, and the aerosol retrieval parameters.

While many progresses were made with past algorithms toward charactering aerosols properties from space, most reliable quantity being retrieved routinely is AOD that is normally characterized at the limited wavelengths or bands. This limitation in part is because that most of these satellite measurements are radiometers with scanning capability in limited number of bands (up to 36 such as MODIS), and in part is restrained by the feasibility to separate the path radiance from surface contributions in various bands (as discussed in the last paragraph). However, a full characterization of aerosol properties requires the retrieval of spectral dependence of aerosol properties (including AOD and absorption), which is also needed in the estimate of radiative forcing of aerosols [25].

This paper presents the second part of a series of studies that aim to develop a hyperspectral remote sensing method for aerosol retrieval from a newly developed GEOstationary Trace gas and Aerosol Sensor Optimization (GEO-TASO) airborne instrument [26]. The GEO-TASO is the airborne version of the upcoming air quality satellite instrument that will measure backscattered ultraviolet (UV), visible (VIS) and near-infrared (NIR) radiation from geostationary orbit, such as Sentinel-4 and Tropospheric Emissions: Monitoring of POllutin (TEMPO) [27,28]. TEMPO was selected as the first Earth Venture Instrument by NASA in 2012 and will be launched between 2019 and 2021 to measure atmospheric pollution for greater North America from space by using hyperspectral UV and visible spectroscopy hourly and with high spatial resolution at 4×4 km^2 [27]. TEMPO will also join Geostationary Environment Monitoring Spectrometer (GEMS) from Korea and Sentianel-4 from Europe as part of the future geostationary satellite constellation [29]. Except for GEO-TASO and TEMPO, other hyperspectral instruments, such as Hyperspectral Infra-Red Imager (HyspIRI), are also under development by NASA [30,31]. Hence, it is necessary to explore and develop algorithms to retrieve aerosols from the hyperspectral measurements.

In the first part of this series of studies, we have developed the theoretical framework of an inversion algorithm to simultaneously retrieve the aerosol properties and surface reflectance. In this framework, it is assumed that surface reflectance spectra can be decomposed into (six) different principal components (PCs) and the wavelength-dependence of aerosol refractive index can be parameterized following a power-law function. These assumptions are generally valid as being supported by the analysis of surface spectra library and Aerosol Robotic Network (AERONET) retrievals [32]. Hence, instead of retrieving surface reflectance at each wavelength, only weight coefficients for each PC are needed to be retrieved.

Based on the framework developed by Hou et al. [32] and the optimal estimation (OE) theory [33], we continue the development of the hyperspectral inversion algorithm by addressing the following feasibility questions: (1) is it possible to obtain the PCs of surface reflectance from the hourly hyperspectral data measured by the instruments (such as TEMPO) in the geostationary (GEO) platform, especially over the surfaces covered by a mixture of different types of canopy? (2) how many and what kind of aerosol parameters can be possibly retrieved together with weighting coefficients for PCs from the hyperspectral data? (3) how can we use GEO's multiple observations with the nearly same Earth-Sun-Satellite geometry in several consecutive days to improve the retrieval? Addressing these questions can provide theoretical guidance in implementing the operational algorithm for aerosol retrieval from GEO-TASO and future geostationary spectrometers.

Table 2
The aerosol scenarios used for synthetic simulations.[a]

Scenarios	$V_{\mathrm{total}}\,(\mu m^3 \mu m^{-2})$	$\mathrm{fmf_V}$	τ_a (550nm)	SSA(550nm)
Fine dominated	0.149 (100%)	0.8 (0.5)	0.8	0.94
Well mixed	0.216 (100%)	0.5 (0.5)	0.8	0.93
Coarse dominated	0.394 (100%)	0.2 (0.5)	0.8	0.92

[a] Bracketed data represent *a priori* errors.

Synthetic data simulated from the Unified Linearized Vector Radiative Transfer Model (UNL-VRTM) [29] is used for the analysis to address the questions above. By using the synthetic data calculated for various surface and atmospheric conditions, we can evaluate our proposed approach and analyze with known 'ground truth' that is used in the generation of synthetic data. We briefly describe the UNL-VRTM and the theoretic framework in Section 2, present our approach and feasibility study of this approach to retrieve PCs from hourly hyperspectral measurements at TOA in Section 3, and conduct the analysis of aerosol information content of these measurements in Section 4. Both Sections 3 and 4 start with the description of background for the method we used. Summary and conclusion are presented in Section 5.

2. Synthetic data

Building on the UNL-VRTM [29], Hou et al. has completed the following developments as part of the theoretical framework for hyperspectral remote sensing of aerosols [32]: (a) integrating the PC analysis (or PCA) of different surface reflectance dataset in the UNL-VRTM, (b) computing the Jacobians of TOA reflectance with respect to (w.r.t.) the PC's weighting coefficients of surface reflectance, with account of the surface bidirectional reflectance distribution function (BRDF), and (c) calculating the Jacobians of TOA reflectance w.r.t the parameters used in the power-law approximation for describing the wavelength dependence of aerosol refractive indices. With these developments, UNL-VRTM is used here to simulate the TOA reflectance and the Jacobians of TOA reflectance w.r.t. the aerosol parameters and the PC's weighting coefficients of surface reflectance for various aerosol conditions, observation geometries and surface types.

In our theoretical framework for hyperspectral remote sensing of aerosols [32], the retrieval parameters contain total aerosol volume (V_{total}), fine volume fraction ($\mathrm{fmf_V}$), particle size distribution parameters ($r^{\mathrm{f}}_{\mathrm{eff}}$, $v^{\mathrm{f}}_{\mathrm{eff}}$, $r^{\mathrm{c}}_{\mathrm{eff}}$, $v^{\mathrm{c}}_{\mathrm{eff}}$) and the coefficients of refractive index ($m^{\mathrm{f}}_{\mathrm{r,0}}$, $b^{\mathrm{f}}_{\mathrm{r}}$, $m^{\mathrm{f}}_{\mathrm{i,0}}$, $b^{\mathrm{f}}_{\mathrm{i}}$, $m^{\mathrm{c}}_{\mathrm{r,0}}$, $b^{\mathrm{c}}_{\mathrm{r}}$, $m^{\mathrm{c}}_{\mathrm{i,0}}$, $b^{\mathrm{c}}_{\mathrm{i}}$) for bimodal (e.g. fine and coarse) aerosols, as well as the PC's weighting coefficients vector $\mathbf{w}$. Here, the superscript f and c represent the aerosol for fine and coarse mode respectively; r_{eff} and v_{eff} are the effective radius and effective deviation respectively, which can be derived from the geometric number mean radius (or volume mean radius) and standard deviation; $m_{\mathrm{r,0}}$, b_{r}, $m_{\mathrm{i,0}}$ and b_{i} are the parameters in the following power-law relationship [34–36] to describe the wavelength-dependence of refractive index as

$$\begin{cases} m_{\mathrm{r}}(\lambda) = m_{\mathrm{r,0}} \cdot \left(\dfrac{\lambda}{\lambda_0}\right)^{-b_{\mathrm{r}}} \\ m_{\mathrm{r}}(\lambda) = m_{\mathrm{i,0}} \cdot \left(\dfrac{\lambda}{\lambda_0}\right)^{-b_{\mathrm{i}}} \end{cases} \tag{1}$$

where λ_0 means the reference wavelength, subscripts r and i denote the real and imaginary part of refractive index, respectively. In this study λ_0=550nm, thus $m_{\mathrm{r,0}}$ and $m_{\mathrm{i,0}}$ are corresponding to the refractive index at 550 nm. Therefore, the state vector for the retrieval can be written as:

$$\mathbf{x} \in \left\{ V_{\mathrm{total}},\quad \mathrm{fmf_V},\, r^{\mathrm{f}}_{\mathrm{eff}},\, v^{\mathrm{f}}_{\mathrm{eff}},\, r^{\mathrm{c}}_{\mathrm{eff}},\, v^{\mathrm{c}}_{\mathrm{eff}}, m^{\mathrm{f}}_{\mathrm{r,0}},\, b^{\mathrm{f}}_{\mathrm{r}},\, m^{\mathrm{f}}_{\mathrm{i,0}},\, b^{\mathrm{f}}_{\mathrm{i}},\, m^{\mathrm{c}}_{\mathrm{r,0}},\, b^{\mathrm{c}}_{\mathrm{r}},\, m^{\mathrm{c}}_{\mathrm{i,0}},\, b^{\mathrm{c}}_{\mathrm{i}},\, \mathbf{w} \right\} \tag{2}$$

Consequently, following the size and refractive index parameters for both coarse- and fine-mode aerosols in the work by Xu and Wang [34] and also listed in Table 3, the synthetic data are calculated by our forward model UNL-VRTM for a typical mid-latitude summer atmospheric profile for various aerosol scenarios (as listed in Table 2). The aerosol properties in Xu and Wang [34] is based on the analysis of AEROENT inversions in Beijing, with single scattering albedo be around 0.92–0.94 in the mid visible. Since in the visible spectrum, the aerosols that are more scattering will have larger impact on the reflectance measured by the satellite, it is expected that the analysis presented here serve as the baseline, and TEMPO may have more information (than what we showed in the paper) for North-American aerosols that are more scattering. Ten different AOD (τ_a) values of 0.05, 0.1, 0.15, 0.2, 0.3, 0.4, 0.5, 0.6, 0.8, 1.0 at 550 nm are considered to represent the various aerosol loadings. For $\tau_a = 0.8$ at 550 nm, the total aerosol volume (V_{total}) can vary from 0.149, 0.216, to 0.394 $\mu m^3 \mu m^{-2}$ for the fine-dominated, well-mixed and coarse-dominated aerosol scenarios, respectively. V_{total} of other AOD value can be gained with linear scaling. The corresponding prior errors of aerosol parameters for the fine and coarse modes are included in Table 3. The fine-mode particles are considered as water-soluble aerosols from OPAC database [37], and the coarse-mode are corresponding to the large spherical particles from the research of Patterson et al. [38] and Wagner et al. [39].

In forward simulations, various solar zenith angles (θ_0), viewing zenith angles ($\theta_v = 0° - 75°$ with the step of 1°) and relative azimuth angles ($\phi = 0° - 180°$ with the step of 1°) are considered. The relative azimuth angle is defined such that $\phi = 180°$ means the observer and Sun are in the same direction and in the same side of the primary plane. Information content analysis shows that the degree of freedom for signal (DFS) of retrieved aerosol parameters vary with scattering angle. However, this variation in terms of the standard deviation of DFS is about 0.09, regardless of the specific aerosol parameters, provided for the same aerosol condition and surface reflectances (as detailed in Section 4.3). Consequently, the following analysis focus on the cases for $\theta_0 = 40°$, $\theta_v = 20°$ and $\phi = 20°$ because DFS results of this observation geometry is representative of the average of DFS values in all possible observation geometries. In other words, if one aerosol parameter could be retrieved with this specific observation geometry, this parameter could also be retrieved at other observation geometries in most cases.

Simulations are conducted for spectral range of 400–700 nm and 400–2400 nm, respectively. The former is the spectral range of TEMPO, while the latter is the spectral range of HyspIRI or any possible future (geostationary) satellite sensors. The simulations are also conducted for various surface conditions with a Lambertian assumption. Four basic surface types (green vegetation, bare soil, rangeland, and concrete) are considered and their corresponding spectra are adopted from the USGS spectral library [40] and the ASTER spectral library [41] (as described in Hou et al. [32]). In addition, we also consider a mixed surface type with reflectance

Table 3
The aerosol parameters for fine and coarse modes.[a]

Mode	$r_{\mathrm{eff}}\,(\mu m)$	v_{eff}	$m_{\mathrm{r,0}}$	b_{r}	$m_{\mathrm{i,0}}$	b_{i}
Fine	0.21 (80%)	0.25 (80%)	1.434 (0.15)	0.016 (0.04)	0.011 (0.01)	-0.266 (0.63)
Coarse	1.90 (80%)	0.41 (80%)	0.549 (0.15)	0.017 (0.04)	0.003 (0.005)	0.625 (0.63)

[a] Bracketed data represent *a priori* errors.

value calculated by equally-weighted reflectance of green vegetation, bare soil, and concrete surface types. We note that the spectral coverage of TEMPO indeed starts from 290 nm and the UV spectral regions has rich information for aerosol height [9,42], but due to the lack of knowledge in wavelength-dependence of surface reflectance and aerosol refractive index in UV spectra as well as the strong gas absorption (by O_3, NO_2 and SO_2) in UV, a combined use of UV and VIS spectra for analyzing the aerosol information content will need a separate study in future.

Fig. 1(a)–(e) respectively shows the surface reflectance for the green vegetation, bare soil, rangeland, concrete, and mixed surface types at wavelengths from 400 nm to 2400 nm. Besides, Fig. 1 (f) presents the total gas transmission in the spectral range of 400–2400 nm with 1 nm interval, and those bands with the gas transmission larger than 94% are selected as the atmospheric window channels in this study. This configuration results in 269 bands in the range of 400–700 nm and 752 bands in the range of 400–2400 nm as the window channels.

Once the forward simulation is conducted, 2.8% Gaussian noises following the calibrating error of GEO-TASO are added to the simulated TOA reflectance to consider the measurement and calibration errors of the sensor. Hereafter, only AOD values at 550 nm are referred, although their spectral dependences are considered in the retrieval.

3. Deriving PCs from TOA reflectance spectra

As a geostationary satellite, TEMPO offers hourly observation for each pixel, enabling more frequent sampling of the spectra at the top-of-atmosphere in conditions with low AOD, and thus better characterizing the surface spectra for that pixel. Indeed, past studies have used the minimum (or second minimum) reflectance at each pixel taken by geostationary imager within a certain time period (~20–25 days) as the surface reflectance in the aerosol retrieval algorithm for GOES [43–48]. Analogically, with TEMPO's observation, a PC analysis of the backscattered spectra in low-AOD conditions can be conducted to obtain the PCs for surface reflectance at each pixel. To evaluate the feasibility of this idea, we first illustrate the relationship between surface and TOA reflectance as a function of AOD and aerosol/surface properties, and then focus on feasibility analysis of deriving PCs from the synthetic data in the condition of small AOD values.

In order to investigate the coupling contribution of aerosol and surface to the TOA measurements for deriving PCs, the forward simulations are also considered in the spectral range of 400–2400 nm with different aerosol model and surface type. Fig. 2(a)–(d) present the separate contributions of Rayleigh scattering, aerosol contribution, surface reflectance (ρ^{s}), and gas absorption to the TOA reflectance (ρ^{TOA}) for four scenarios: the combination of two aerosol scenarios (respectively for fine-mode and coarse-mode aerosol dominated) over two surface types (green and yellow vegetation). In those four cases AOD at 550 nm is assumed 0.4. In reference to the reflection of surface, the TOA reflectance can be reduced by absorption with certain gases, and enhanced by scattering with the gas molecules and aerosol particles. These effects combine to produce the TOA reflectance spectral curve illustrated in Fig. 2. The pronounced absorption features near 1.18, 1.4 and 1.9 μm, cased by water vapor and/or carbon dioxide, reduce incident and reflected energy almost completely, so little useful information could be obtained from the spectral bands in these regions. In this region, O_3 has a weak absorption (Chappuis band in which absorption is about a factor of 10^4 smaller than in the UV) and O_2 has strong absorption in around 0.688 and 0.763 μm [49].

Rayleigh scattering's contribution to ρ^{TOA} dominates in the blue spectrum (400–450 nm) and decreases sharply with the increase

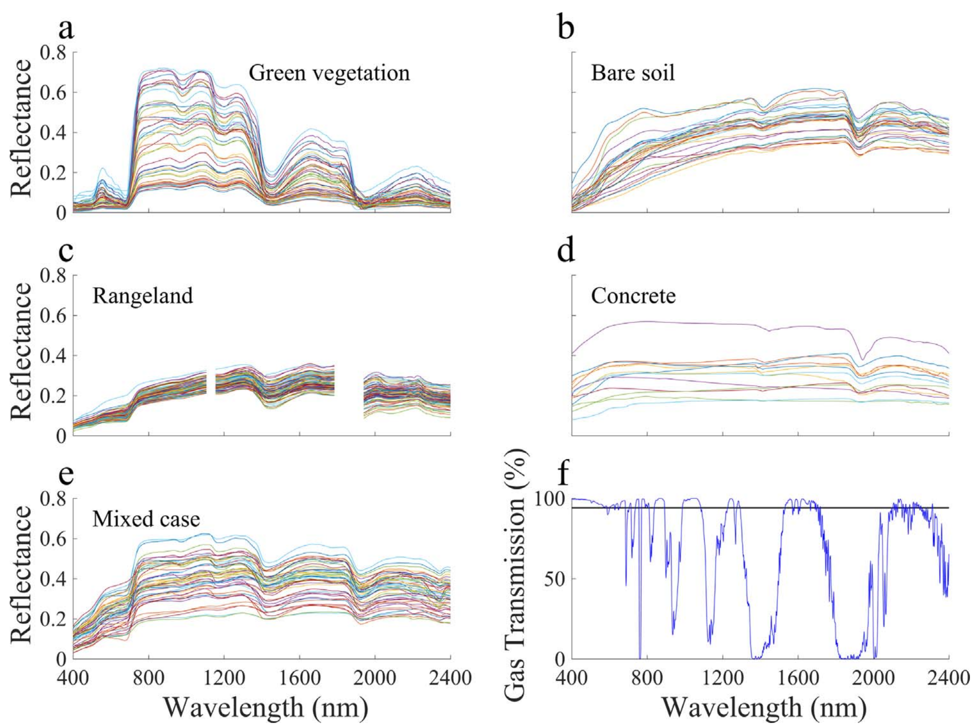

Fig. 1. The spectral datasets and simulated gas transmission by UNL-VRTM. (a–e) Spectra of surface reflectance for various surface types as indicated in the figure, in which the green vegetation (a) and rangeland (c) datasets are adopted from the USGS spectral library, bare soil (b) dataset is adopted from the ASTER spectral library and further smoothed, concrete (d) dataset is adopted from both of the spectral libraries, and the mixed case (e) dataset is equally weighted by the surface reflectances of green vegetation, bare soil, and concrete. Besides, panel (f) plot the two-way total gas transmission (from TOA to the surface then to the TOA) simulated by the UNL-VRTM with θ_0=40° and θ_v=20°, in which the black horizontal line is used to distinguish the window channel bands with the gas transmission larger than 94%.

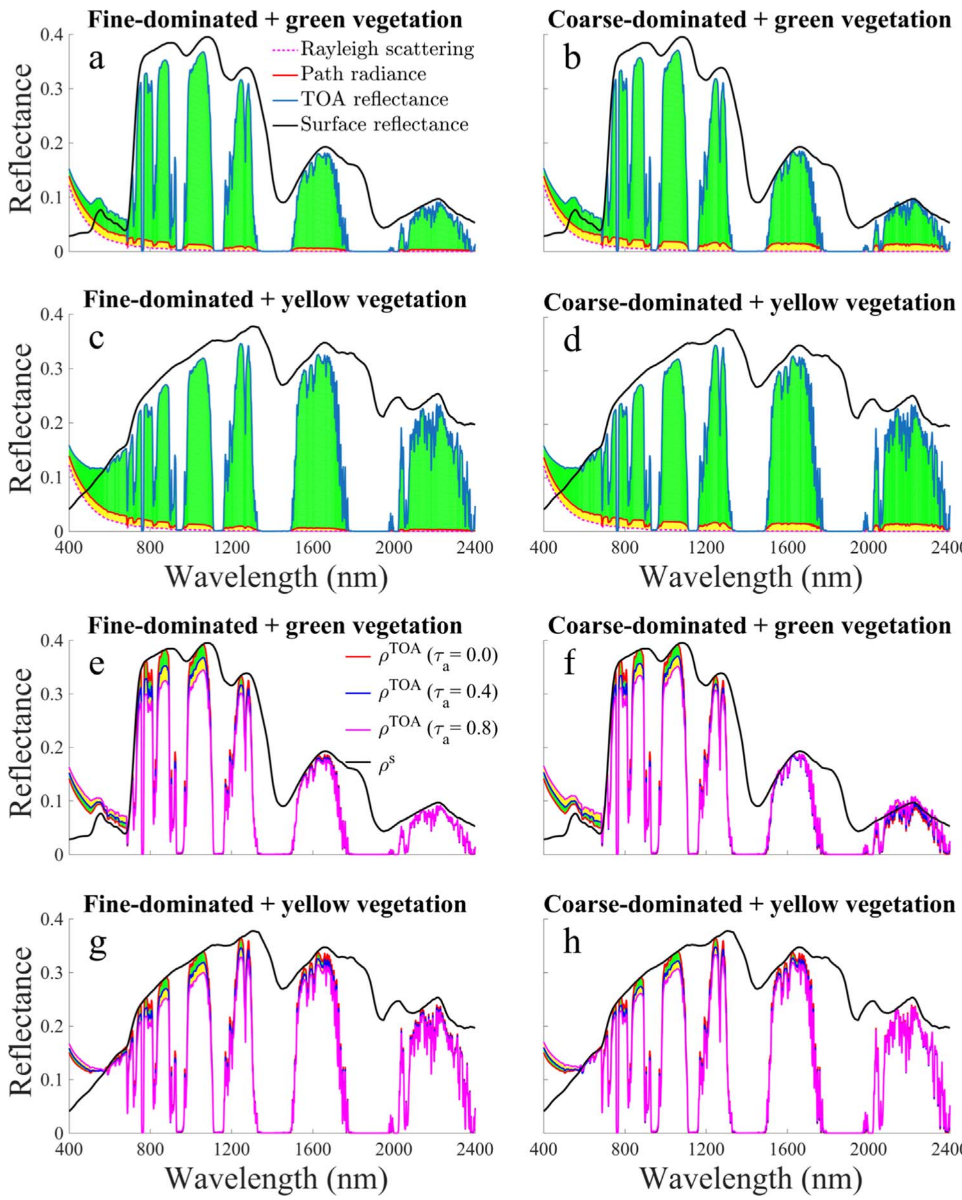

Fig. 2. Panels (a–d) present the contribution of Rayleigh scattering, path radiance and surface reflectance ρ^s to the TOA reflectance ρ^{TOA} simulated by UNL-VRTM with consideration of gas absorption and AOD τ_a=0.4 at 550 nm. Each panel corresponds to a combination of one aerosol model (fine-dominated or coarse-dominated) and one surface type (green vegetation or yellow vegetation). Spaces between adjacent spectral curves are shaded with different colors to highlight the separated contributions, in which yellow shaded region represents the contribution of aerosol only (including the gas absorption), and green shaded region represents the coupled contribution of surface and atmosphere to TOA reflectance. Correspondingly, panels (e–h) present the spectra of ρ^{TOA} with the different AOD τ_a=0,0.4,0.8, in which the yellow and greed shaded parts are used to highlight the scattering or absorption contributions with the increased AOD.

of wavelength. As the wavelength increases, the coupled contribution of surface and atmosphere (e.g., green shaded region) accounts for over 90% of TOA reflectance in atmospheric window channels. The wavelength-dependence of this coupled contribution, however, depends on the aerosol particle size as well as the surface reflectance spectra. In principle, TOA reflectance increases when surface reflectance increases and/or aerosol scattering increases. In each of those four cases respectively for two surface types (Fig. 2a–d), the inset figure shows that for the same AOD and surface reflectance, the difference of ρ^{TOA} for different aerosol scenarios can be up to 2.0%. For the same surface type, it is found that the coupled contribution of surface and atmosphere has about 4.0% difference between the atmospheres of fine-mode dominated aerosols and coarse-mode dominated aerosols.

Compared with the contribution from atmosphere-surface coupling, the contribution solely from aerosol (yellow shaded region in Fig. 2) to the TOA reflectance is very small. For the same surface type, the contribution of coarse-mode dominated aerosols is larger than that of fine-mode dominated aerosols in atmospheric window channels from 550 nm to 2400 nm. Especially, in spectral range of 2100–2400 nm, the contribution of coarse-mode dominated aerosols is 4–5 times larger than the contribution of fine-mode dominated aerosol. Therefore, knowledge or characterization of surface reflectance in these wavelengths are needed to retrieve properties of large aerosol particles [50]. From another perspective, however, the strong influence of surface in radiative transfer also renders strong similarities between ρ^{TOA} spectra and ρ^s spectra, except in spectral regions of blue bands where surface reflectance is low and Rayleigh scattering is significant. It is foreseeable that ρ^{TOA} spectra after the correction of Rayleigh scattering can be used to derive the spectral variation of ρ^s, and hence, frequent samples of ρ^{TOA} for a fixed location at a fixed view angle can

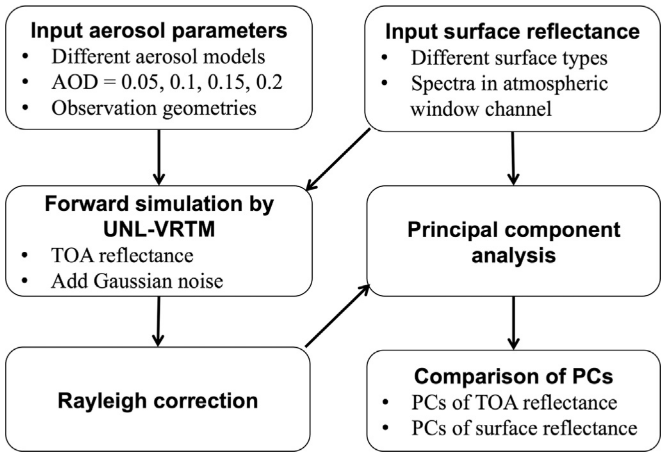

Fig. 3. Flowchart of testing the feasibility to extract the PCs from TOA reflectance.

be used to derive the PCs that account for the spectral variation of ρ^{s}.

To further study the spectral similarities between ρ^{TOA} data (after Rayleigh correction) and ρ^{s}, we also simulate ρ^{TOA} for AOD values of 0, 0.4, and 0.8. As seen from Fig. 2(e)–(h), aerosol scattering leads to increase of reflectance in visible bands; the higher AOD value yields higher ρ^{TOA}. But, as surface reflectance increases, ρ^{TOA} is smaller than ρ^{s} at spectral wavelengths larger than 700 nm because aerosol absorption is amplified due to the larger surface reflectance (and stronger coupling between surface reflectance and atmosphere). It is interesting that in atmospheric window channels in the near-infrared region (such as 1640 and 2200 nm), the ρ^{TOA} and ρ^{s} reflectance are nearly equal regardless of the surface type or AOD [51,52]. Hence, Fig. 2(e)–(h) show that ρ^{TOA} spectra (in most wavelengths of window channel) can be used to derive the spectral variation of ρ^{s} after Rayleigh correction.

Fig. 3 gives the flowchart of testing the feasibility to identify PCs of surface reflectance spectra from the TOA reflectance spectra. For the forward simulation by UNL-VRTM, different aerosol models (fine-dominated, well-mixed, and coarse-dominated), small AODs (τ_a= 0.05, 0.1, 0.15, 0.2) and representative observation geometry (θ_0 = 40°, θ_v=20°, ϕ = 20°) are considered, as well as the surface reflectance spectra in atmospheric window channel with different surface types (green vegetation, bare soil, rangeland, concrete and mixed case). After that, the simulated TOA reflectance spectra with 2.8% Gaussian noise are corrected for the Rayleigh scattering according to the surface pressure, as described in Bodhaine et al. [53] and Tomasi et al. [54]. Only those Rayleigh-corrected TOA spectra in the window channel are used for the analysis of surface PCs.

Fig. 4 displays the scatterplot of 1st–6th PCs derived from TOA reflectance versus those used in the forward simulation ("truth") in the spectral range of 400–2400 nm respectively for 5 different surface types. In general, the derived PCs agree well with the "truth" at each wavelength with coefficient of determination R^2 larger than 0.99 in most cases. Similar agreements are also found for these cases in the spectral range of 400–700 nm (R^2>0.99 in most cases). In the practical retrieval, because land surface usually is a mixture of different surface types, the true PCs of surface reflectance cannot be exactly obtained, and thus those derived PCs from TOA can be used with the consideration of uncertainties in these PCs. As in the discussion [32], surface reflectance can be decomposed in different PCs, and these 6 PCs can reconstruct the true surface reflectance with averaged relative error of 1%. Nevertheless, based on the theoretical analysis here, if we use these PCs derived from TOA spectra in low AOD conditions to reconstruct the surface reflectance, the reconstructed surface reflectance have the averaged relative error of 1% compared with the results reconstructed by the PCs of true surface reflectance.

4. Information content analysis of aerosols

Previous analyses of aerosol information content from various satellite measurements are briefly summarized in Section 4.1. The sequential forward selection method is then used together with the DFS analysis to obtain the common bands in the spectral range of 400–700 nm and 400–2400 nm respectively for different aerosol models and surface types in Section 4.2. Using these common bands (instead of all window bands) can facilitate the retrieval process by lowering the computational cost. Subsequently, the information content analysis for GEO-TASO and the geostationary satellites such as TEMPO are conducted for single measurement at these common bands in the spectral range of 400–700 nm in subsection 4.3. At last, the constraints of multiple measurements from geostationary satellites at the same time in the consecutive days are presented in Section 4.4.

4.1. Background

Following the methodology of Rodgers [33], the information content analysis can be conducted to exploit the spectrometer measurements for aerosol parameters retrieval, and the number of degrees of freedom for signal (DFS) is usually used to represent the number of parameters that can be retrieved independently from TOA reflectance measurements, provided that the surface reflectance and the prior error of retrieval parameters are characterized. One important metric in the information content analysis is the averaging kernel matrix **A**, which characterizes the changes in the retrieved stated vector $\hat{\mathbf{x}}$ to changes in the true state vector **x**, that is

$$\frac{\partial \hat{\mathbf{x}}}{\partial \mathbf{x}} = \mathbf{A} = \mathbf{GK}, \tag{3}$$

in which the retrieval Gain matrix

$$\mathbf{G} = (\mathbf{K}^T\mathbf{S}_\epsilon^{-1}\mathbf{K} + \mathbf{S}_a^{-1})^{-1}\mathbf{K}^T\mathbf{S}_\epsilon^{-1}, \tag{4}$$

where the superscript "T" and "−1" represent the transpose and inverse operator of matrix, respectively, $\mathbf{S}_\epsilon$ is the observation error covariance matrix, $\mathbf{S}_a$ is the error covariance matrix of the *a priori* estimate $\mathbf{x}_a$, $\mathbf{K} = \frac{\partial \mathbf{F}(\mathbf{x})}{\partial \mathbf{x}}$ means the Jacobian matrix of forward model $\mathbf{F}(\mathbf{x})$ with respect to **x**. The trace of **A** describes the amount of independent pieces of information from the retrieval of measurements, also called the degrees of freedom for signal (DFS). Correspondingly, the *a posteriori* error covariance matrix $\hat{\mathbf{S}}$, is defined as

$$\hat{\mathbf{S}} = (\mathbf{K}^T\mathbf{S}_\epsilon^{-1}\mathbf{K} + \mathbf{S}_a^{-1})^{-1}, \tag{5}$$

which represents the statistical uncertainties in retrieved $\hat{\mathbf{x}}$ caused by measurement noise and smoothing [55]; the diagonal elements of $\hat{S}^{\frac{1}{2}}$ are the posterior errors. As for the observation error covariance matrix $\mathbf{S}_\epsilon$, it contains two parts:

$$\mathbf{S}_\epsilon = \mathbf{S}_y + \mathbf{K}_b\mathbf{S}_b\mathbf{K}_b^T, \tag{6}$$

in which $\mathbf{S}_y$ is the instrumental error covariance matrix, $\mathbf{S}_b$ represents the error covariance matrix for a vector **b** of forward model that are not contained in **x** but quantitatively influence the measurements, $\mathbf{K}_b$ means the Jacobians matrix of measurements **y** w.r.t. **b**.

Many studies have evaluated the information content from the satellite measurements of the solar backscatter on aerosol in the spectral range of UV to near infrared [56]. For example, 1–2 parameters of the particle size distribution could be retrieved from MODIS using the multi-bands from 470 nm to 2130 nm [57], and

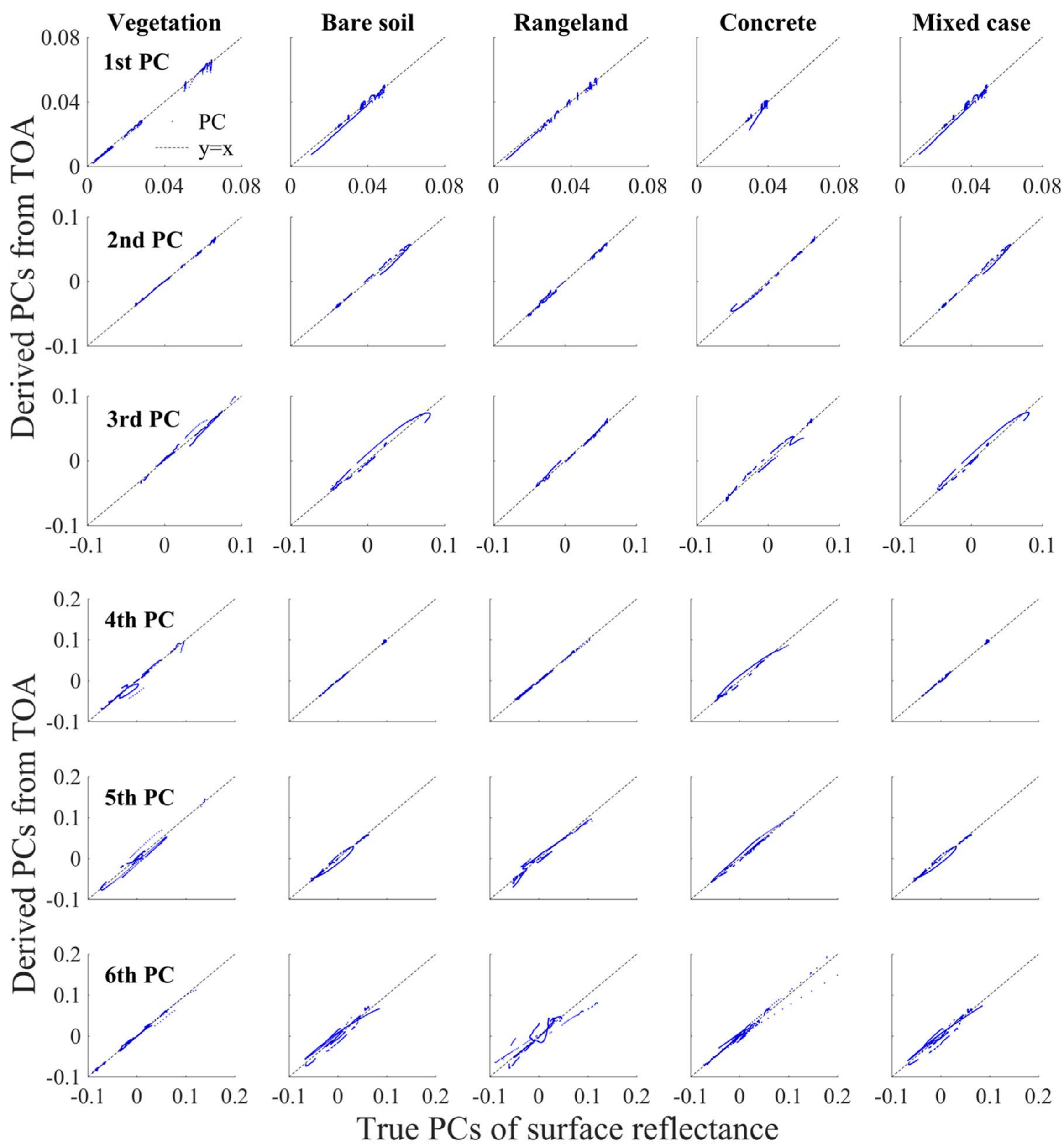

Fig. 4. Scatterplot of the 1st to 6th derived PCs from TOA versus true PCs for different surface types (green vegetation, bare soil, rangeland, concrete, mixed case respectively) with 4 small AOD cases ($\tau_a = 0.05, 0.1, 0.15, 0.20$) and one representative observation geometry (θ_0=40°, θ_v=20°, ϕ = 20°), in which the blue dot represent the PC value at each window channel band in the range of 400–2400 nm. For different surface types, there are 50 green surface spectra, 30 bare soil spectra, 70 rangeland spectra, 13 concrete spectra and 50 mixed spectra used respectively for simulations. (For interpretation of the references to color in this figure legend, the reader is referred to the web version of this article.)

3.5 to 5 independent pieces of information can be obtained from the intensity measurements of GOME-2 from 300 nm to 800 nm [58]. Veihelmann et al. [56] also found 2–4 DFS for aerosol parameters from OMI reflectance measurement, and the information content further depends on the observation geometry and the surface type. Besides, there are 2–4 parameters (including AOD, aerosol type and surface reflectance) that could be retrieved from 10 synergetically-selected bands of AASTR and SCIAMACHY by SYNergetic AErosol Retrieval (SYNAER) algorithm in the range of 415–675 nm [59,60]. In addition, the combined retrieval method of aerosol and greenhouse gas has been investigated by Frankenberg et al. [55]. They showed that the ability to retrieve aerosol properties in terms of DFS could be enhanced greatly by 2–3 with multiple satellite viewing angles simultaneously. Furthermore, retrieval of aerosol microphysical properties form AERONET are also discussed by Xu and Wang [34], and the information content analysis results show that adding polarization measurements can increase the DFS by $2-5$ with the solar principal plane radiances and polarization. In our study, we analyze the information content for aerosol parameters for a large number of scenarios for a given observation geometry, different aerosol models, and surface types, thus evaluating what kinds of aerosol parameters could be retrieved from hyperspectral remote sensing.

Due to the dense measurements with hundreds of spectral channels in the visible to near-infrared wavelengths, hyperspectral images contain more aerosol and surface information than traditional multispectral instruments. However, as the spectral interval between the adjacent bands in hyper-spectra is very fine, and the correlation between them is inevitable, there should be considerable redundancy in hyperspectral data [61]. Therefore, band selection methods based on information content analysis are needed to reduce the dimensionality of hyperspectral imagery in the inversion, and then the efficiency of aerosol retrieval could be greatly improved with those best bands containing most of information content. Among a large group of band-selection algorithms for hyperspectral data, we use the forward-searching strategies such as the sequential forward selection (SFS) and sequential forward floating selection (SFFS) [62] to test all the possible combinations of hyperspectral bands.

4.2. DFS analysis for sequential forward selection of bands

Corresponding to our inversion theoretical framework, the aerosol parameter and PC' weighting coefficients ($\mathbf{w}$) of surface reflectance need to be retrieved simultaneously. Thus, in the information content analysis, common bands for retrieval are selected according to DFS values for aerosols in these bands. The state vector can be set as

$$\mathbf{x} = \left[V_{\text{total}},\ \text{fmf}_V,\ r_{\text{eff}}^{f},\ v_{\text{eff}}^{f},\ r_{\text{eff}}^{c},\ v_{\text{eff}}^{c},\ m_{r,0}^{f},\ b_r^{f},\ m_{i,0}^{f},\ b_i^{f},\ m_{r,0}^{c},\ b_r^{c},\ m_{i,0}^{c},\ b_i^{c},\ \mathbf{w} \right]^T. \tag{7}$$

The error matrix of state vector follows Hou et al. [32], and the standard errors of weighting coefficients are also contained as

$$\mathbf{S}_a = \text{diag}\left(\left[\sigma_{V_{\text{total}}}^2,\ \sigma_{\text{fmf}_V}^2,\cdots,\ \sigma_{m_{i,0}^c}^2,\ \sigma_{b_i^c}^2,\ \sigma_{w1}^2,\ \cdots,\ \sigma_{w6}^2 \right]^T \right), \tag{8}$$

in which, the prior errors corresponding to those parameters have been listed in Tables 2 and 3. For the instrument error matrix,

$$\mathbf{S}_y = \text{diag}\left(\left[\left(e_1 \times I_{\lambda 1}\right)^2,\cdots,\left(e_d \times I_{\lambda_d}\right)^2 \right]^T \right), \tag{9}$$

where diag$(\cdots)$ denotes to assign a vector on the main diagonal of matrix, e_i represents the relative error of measurements at each wavelength. Following the calibrating error of GEO-TASO, e_i is set about 2.8%; here $i = 1,\cdots, d$, where d represents the number of wavelength bands used in analysis. For the calculation of information content with selected aerosol parameters, the prior errors of the parameters in vector $\mathbf{b}$ corresponding to the state vector are based on the AERONET retrieval errors following the work of Dubovik et al. [63].

Combined with the information content analysis and total aerosol DFS result, the sequential forward selection (SFS) method can be used to select the best subset of the bands for retrieval. Given a band set $B = \{\lambda_1, \cdots, \lambda_d\}$ in the atmospheric window, a subset $\hat{B}_M$ is found to maximize the total DFS results as

$$\hat{B}_M = \left\{ \lambda_{i_1}, \cdots, \lambda_{i_M} \right\} = \arg\max_{M,\, i_M} DFS \left\{ \lambda_i i = 1,\cdots, d \right\} \tag{10}$$

here the operator "arg max" stands for the argument of the maximum, and M is the number of selected bands subset. SFS algorithm usually starts from an empty or a predefined bands subset, and sequentially adds the band λ^+ that maximize $DFS\left(\hat{B}_k+\lambda^+\right)$ when combined with the bands $\hat{B}_k$ that have already been selected. The SFS's steps are as the following:

Step 1: start with the predefined band set $\hat{B}_0$;
Step 2: select the next best band $\lambda^+ = \arg\max_{b \notin \hat{B}_k} DFS\left(\hat{B}_k+\lambda\right)$;
Step 3: Update the bands subset $\hat{B}_{k+1} = \hat{B}_k+\lambda^+$, and $k = k + 1$;
Step 4: Go to step 2 until $k = M$.

In this study, the predefined band set is always started with following the central wavelength of MODIS [4], in which $\hat{B}_0 = \left\{ 466, 553, 646\text{nm} \right\}$ for the range of 400–700 nm, and $\hat{B}_0 = \left\{ 466, 553, 646, 855, 1243, 1632, 2119\text{nm} \right\}$ for the range of 400–2400 nm. The main disadvantage of SFS is that once the band is selected, it can't be removed any more. Other feature selection algorithms such as the plus-L minus-R selection or sequential floating selection can avid this disadvantage. In this study, only the SFS method is applied for band selection.

Fig. 5 shows the total DFS of aerosol retrieval as a function of the number of wavelength sorted by SFS in the spectral range of 400–700 nm and 400–2400 nm, respectively. The corresponding total DFS of 6 PCs' weighting coefficients also have the similar trend, and these figures are not shown here. With the growing number of sorted wavelength bands, the total DFS value increases relatively fast for the first 10% of bands; after that, DFS grows slowly and approaches its maximum. In addition to the number of selected bands, DFS values also depend surface type, aerosol model, and aerosol loading. Among those five typical surface types, the maximum values of DFS are over green vegetation, which corresponds to the surface type for "dark target" algorithm. For those sparsely green vegetated surfaces, including bare soil, rangeland and mixed case, the information content for aerosols are smaller and have similar DFS values. For the bright urban (mainly concrete) surface, DFS value is decreased by 2 as compared to that for the green vegetated surface. The DFS for coarse-mode dominated aerosols is usually 1 larger than the that of fine-dominated aerosols for the same AOD and surface type. The DFS value for well-mixed case is between the results of fine-dominated and coarse-dominated aerosol model. We note that a known fine-mode aerosol volume fraction fmf_V with associated uncertainty is needed to generate synthetic measurements, and thereby the information content analysis is conducted through linearization of radiative transfer calculation at this tangent point for fmf_V. This is a common practice in the framework of optimization and information content analysis, and the underlying assumption is that with many case analysis for different tangent points, the results will be robust to reveal the information content in the measurements [29]. In the practical inversion process, fmf_V is an unknown parameter in the state vector that is to be retrieved from spectral measurements of radiances. A first guess of fmf_V for practical retrieval can be obtained from AERONET [64], aerosol climatology [65], or chemistry transport model simulation [48,66], etc.

For the total DFS values calculated by all the bands in the atmospheric window channel, in most cases, the contribution of the first 20% sorted window channels can account for at least 90% of total DFS, regardless of surface types or aerosol models. Thus, we have totally 30 test cases here, including the combinations of 5 different surface types, 3 different aerosol models, and 2 different AOD cases ($\tau_a = 0.2, 0.8$). In other words, we can use those 20% sorted bands to retrieve 90% of aerosol information. However, those top 20% bands (in terms of DFS) do vary with surface types, and they are not the same for all 30 test cases. Hence, we need to find a method to determine those common bands for retrieval.

In those 30 test cases, considering the sorted top 20% and 36% window channel bands for each case, we calculate the frequency of each band, and select those bands corresponding to the frequency larger than 20, which is 66.7% of the number of total test cases. In this way, Fig. 6 shows the selected common bands for retrieval over the spectral ranges of 400–700 nm and 400–2400 nm. From the first 20% sorted window channel bands by SFS, we found that at least 8% channel bands could be selected as the common bands, which can account for about 80% of total information content; while from the first 36% sorted window channel bands, at least 20% window channel bands with respect to those sorted bands

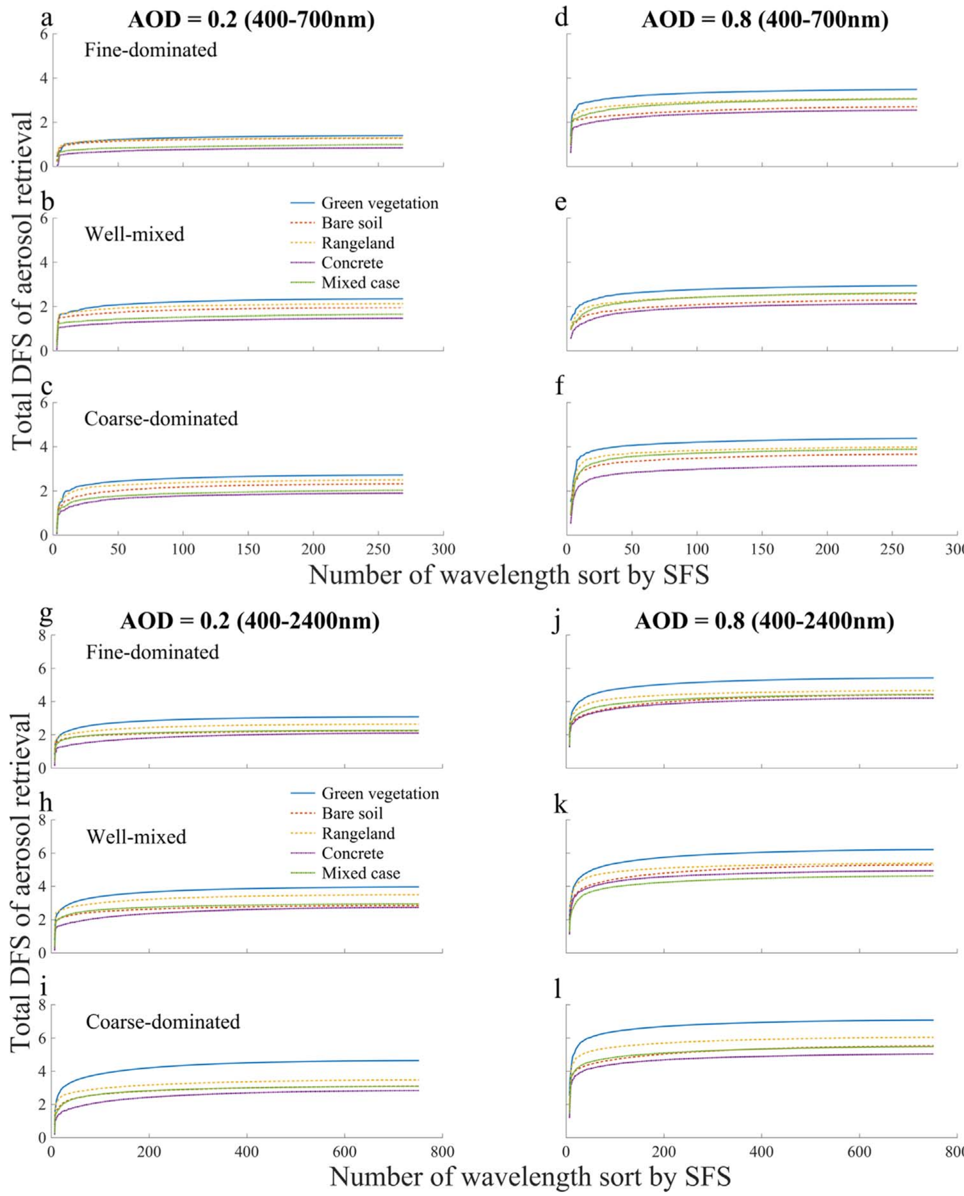

Fig. 5. Total DFS of aerosol retrieval as a function of the number of atmospheric window channels sort by sequence forward selection (SFS) method in 400–700 nm (a–f) and 400–2400 nm (g–l), respectively, for the case of 6 PC's coefficients of surface reflectance are retrieved with the aerosol parameters together. The band set starts with $\{466, 553, 646\text{nm}\}$ for the range of 400–700 nm, and $\{466, 553, 646, 855, 1243, 1632, 2119\text{nm}\}$ for the range of 400–2400 nm. Left column is for cases of AOD = 0.2 and right column for AOD = 0.8.

could be obtained as the common bands, and account for more than 90% of total DFS. These results suggest that there are available common bands for retrieving aerosol properties, regardless of varied surface types and aerosol models.

In order to study the information content and the hyperspectral retrieval algorithm for GEO-TASO and TEMPO, we focus on the visible bands in the this study, and use those selected top 20% window channel bands as the common bands (about 50 wavelengths) over the spectral ranges of $400-700$ nm to analyze the information content. When only 50 common bands are considered, 4 PCs can cover more than 99.9% of variance contribution and the averaged relative error of reconstructed reflectance is smaller than 1% in most cases for the typical spectral datasets, including the green vegetation, bare soil, rangeland, concrete, and mix surface types. Therefore, in addition to retrieve aerosol parameters, only 4 PCs' weighting coefficients need to be retrieved from 50 common bands in the visible spectral range. Hereafter, this strategy is used in the aerosol information content and surface content analysis for individual and multiple measurements respectively in Sections 4.3 and 4.4. Except for V_{total} and fmf_V, we only consider to retrieve the parameters for the aerosols that are in the dominate mode (such as r_{eff}, $m_{\text{r},0}$, b_r for fine-dominated or coarse dominated cases) due to the limited information; for the well-mixed case, these parameters of fine-dominated model are considered.

4.3. DFS analysis for individual observation in common bands

In order to determine what kind of aerosol parameters could be combined for the retrieval with 4 PC's weighting coefficients by common bands, we take a serial selection approach. We first consider to retrieve just one parameter (such as V_{total}) provided the DFS for that retrieval is the largest and above 0.5. Indeed, we don't consider that parameter to be retrieved if DFS is less than 0.5. Once the first retrievable parameter is selected, a second parameter will be added into DFS analysis provided that the added aerosol

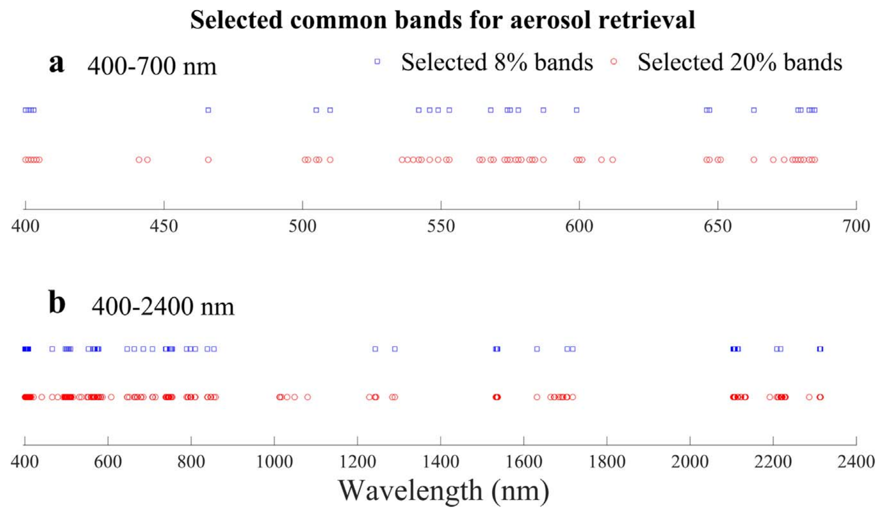

Fig. 6. Common spectral bands for aerosol retrieval selected by the SFS method for spectral ranges of 400–700 nm (a) and 400–2400 nm (b). Blue and red dots represent selections of 8% and 20% of window channel bands, respectively.

parameter has DFS value larger than 0.5 and has the largest the DFS in the remaining parameters. We repeat these criteria to sequentially select and add the parameter into the state vector for the retrieval, and thereby the appropriate retrieval combinations could be determined.

For the individual observation, fifty green spectra from vegetated spectral dataset and ten AOD values (τ_a = 0.05, 0.1, 0.15, 0.2, 0.3, 0.4, 0.5, 0.6, 0.8, 1.0) are considered, thus the averaged DFS and standard deviation (error bar) could be calculated. Fig. 7 shows the averaged DFS of retrieving aerosol parameters for individual observation with different aerosol models. When AOD $\tau_a \geq 0.2$, one aerosol parameter (V_{total}) can be first retrieved with the mean DFS values of 0.94, 0.87, and 0.88 respectively for fine-dominated, well-mixed, and coarse-dominated aerosol conditions (Fig. 7a). As we consider to add one aerosol parameter in sequence with V_{total}, Fig. 7b illustrates the total DFS for V_{total} and dominated-mode r_{eff} when $\tau_a \geq 0.5$. If $\tau_a < 0.5$, DFS of r_{eff} is small than 0.5 in most cases, hence still cannot be retrieved with V_{total}. Similarly, Fig. 7c shows the total DFS for V_{total} and fmf_V when $\tau_a \geq 0.5$. Here, the parameter fmf_V only could be retrieved together with V_{total} where atmosphere is dominated by fine-mode aerosols. For other aerosol parameters, the DFS results are all smaller than 0.5 and cannot be retrieved together with V_{total}, regardless of limited information content. In most cases, the total DFS for the weighting coefficients of four PCs are larger than 0.85 (figure not shown).

Therefore, for the small AOD case ($\tau_a < 0.2$), deriving V_{total} with four weighting coefficients is still a difficult task, even over green vegetation surface; while for the medium or large AOD case ($\tau_a \geq 0.5$), the information content can be slightly richer and retrieval of fine-mode r_{eff} might be possible.

All the DFS analysis above is shown for observation geometry of $\theta_0 = 40°$, $\theta_v = 20°$, and $\phi = 20°$. Can the DFS result of this

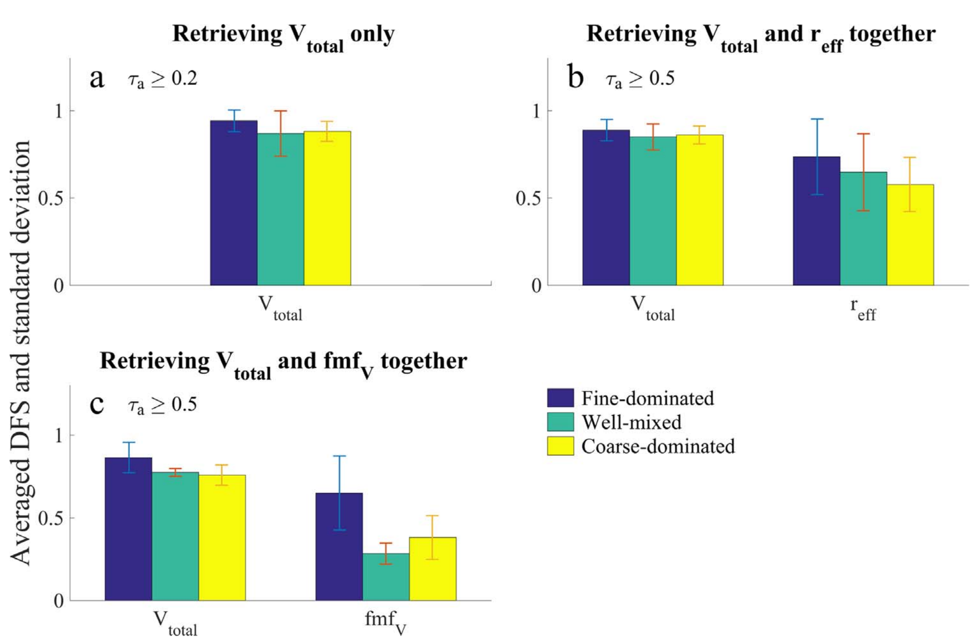

Fig. 7. Mean and standard deviation of DFS for the retrieval of aerosol parameters with 4 PC's weighting coefficients by the common bands of observation in the range of 400–700 nm. Panel (a) is for retrieving one aerosol parameter V_{total} when $\tau_a \geq 0.2$, panel (b) is for simultaneous retrieval of V_{total} and r_{eff} of the dominated aerosol mode when $\tau_a \geq 0.5$, and panel (c) represent the simultaneous retrieval of V_{total} and fmf_V when $\tau_a \geq 0.5$. Aerosol models are indicated by blue for fine-dominated, green for well-mixed, and yellow for coarse-dominated. Here, the dominated-mode r_{eff} represent r_{eff}^f for fine-dominated and well-mixed cases, and represent r_{eff}^c for coarse-dominated case, so as the dominated-mode $m_{r,0}$, b_r presented in Figs. 10–12. (For interpretation of the references to color in this figure legend, the reader is referred to the web version of this article.)

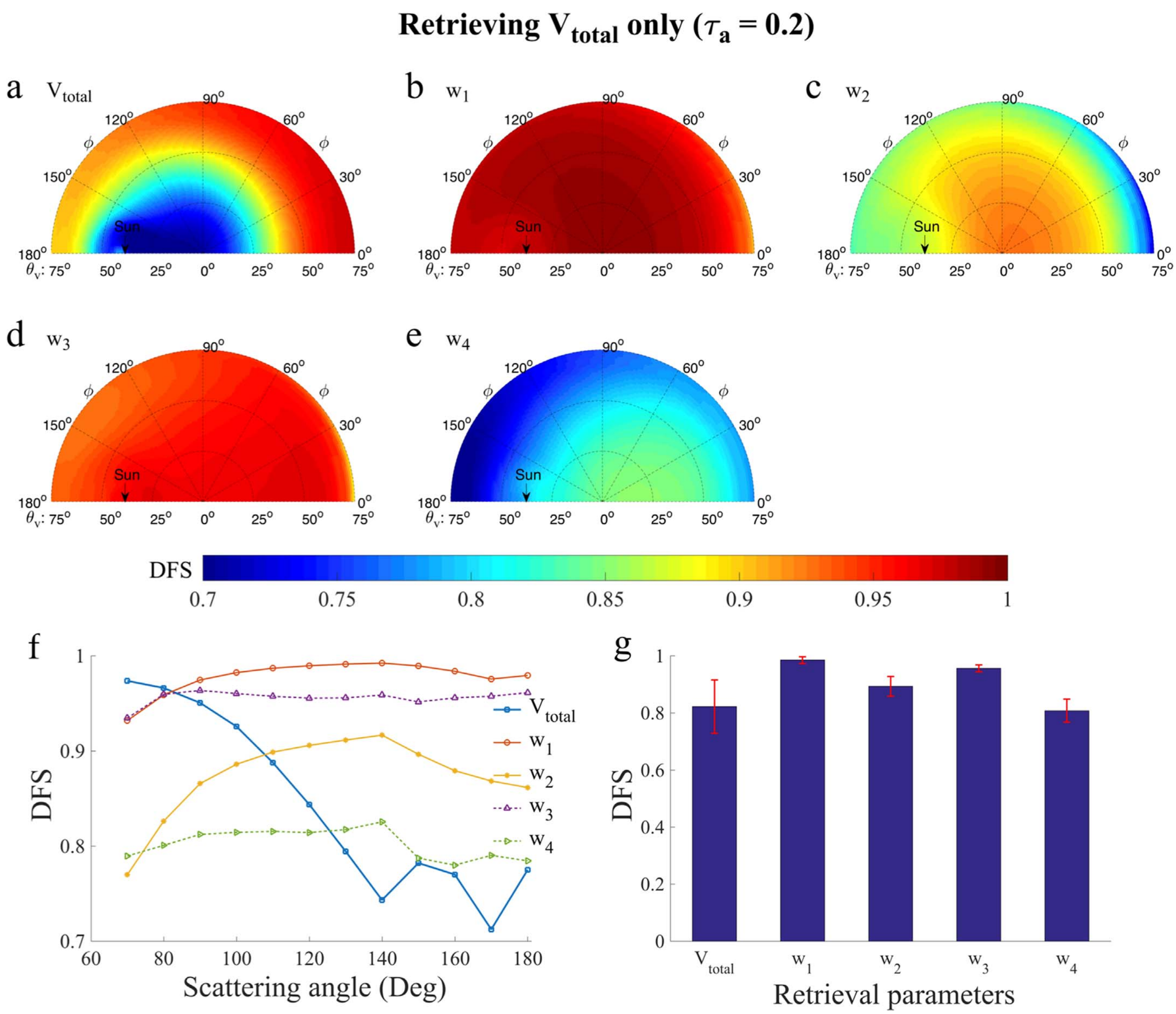

Fig. 8. DFS results of retrieving one aerosol parameter (V_{total}) and 4 PC's weighting coefficients (w_1–w_4) at various observation geometries for the small AOD case (τ_a=0.2) by the selected common bands in 400–700 nm with fine-dominated aerosol. Panels (a–e) are the polar-plots of DFS for V_{total}, w_1, w_2, w_3, w_4, respectively. In these polar plots, radius represents θ_v, polar angle indicates ϕ, and forward simulations are for θ_0=40°. Panel (f) shows the DFS as a function of scattering angle for those five retrieval parameters. Panel (g) is the histogram of mean and standard deviation of DFS of those five retrieval parameters for considered observation geometries.

observation geometry represent those results of other geometries? Fig. 8 shows the polar-plot of DFS for the small AOD case ($\tau_a = 0.2$) with fine-mode aerosol dominated case for retrieving one aerosol parameter only. For the retrieval of V_0, DFS generally decrease with the increasing of scattering angle; when the scattering angle Θ is around 170°, the DFS of V_0 reaches the minimal value, and the standard deviation of DFS is about 0.09 for all of the scattering angles. For the retrieval of PC's weighting coefficient, the DFS shows little variation with different observation geometries, and the standard deviation of each weighting coefficient is all smaller than 0.04.

Contrary to Fig. 8, Fig. 9 shows the polar-plot of DFS for the $\tau_a = 0.8$ for the retrieval of two aerosol parameters together (V_0 and r_{eff}). The DFS value of each retrieval aerosol parameter also decreases with the increasing of scattering angle, and reaches the minimal at scattering angles around $\Theta = 170°$; the standard deviation is all smaller than 0.03. The DFS for PC's weighting coefficients are similar as Fig. 8, and the figures are not show here.

Consequently, information content analysis shows that the DFS of retrieved aerosol parameters vary with scattering angle. However, this variation in terms of the standard deviation of DFS is smaller than 0.1, and DFS results of given observation geometry ($\theta_0 = 40°$, $\theta_v = 20°$, and $\phi = 20°$) can be representative of the mean DFS values in all possible observation geometries regardless of the specific aerosol parameters, provided for the same aerosol condition and surface reflectance. Therefore, based on Fig. 8 and Fig. 9, we can validate that the DFS result in the observation geometry that we used in the above analysis ($\theta_0 = 40°$, $\theta_v = 20°$, and $\phi = 20°$) can represent the results of other geometries.

4.4. DFS results for multiple observations in common bands

For geostationary satellites such as TEMPO, the TOA spectra can be acquired for the same place at a given local time with a constant view angle and nearly the same solar angle in multiple adjacent days. Because the surface reflectance changes in a much slower pace than the aerosol loading (or AOD) at the same location

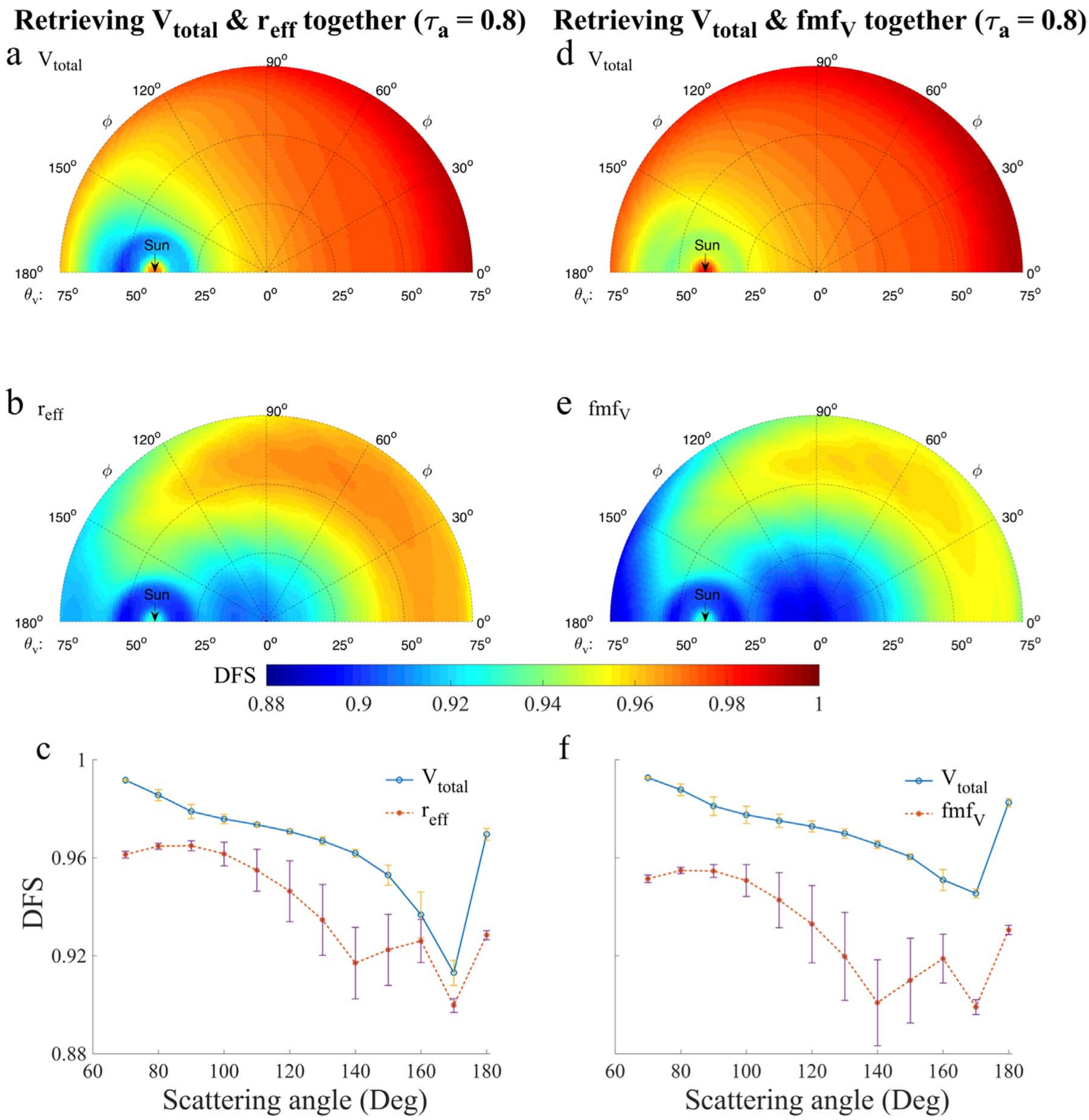

Fig. 9. Similar to Fig. 8, but for DFS results of retrieving two aerosol parameter ($\{V_0, r_{eff}\}$ or $\{V_0, fmf_V\}$) together with four PC's weighting coefficients (w_1–w_4) for the large AOD case (τ_a=0.8) using the selected common bands in 400–700 nm with fine-dominated aerosol. Left panel is for V_0 & r_{eff} case, while right panel is for V_0 & fmf_V case. Panel (c) and (f) represent the averaged DFS of retrieved aerosol parameters and standard deviation bar as a function of scattering angle. The DFS of w_1–w_4 is similar to the results shown in Fig. 8 and are not shown here.

[67], we can use observation at the same time in multiple days to simultaneously retrieve the parameters of aerosol and surface reflectance. Hence, we assume that the parameters of particle size distribution $\left(r^f_{eff}, v^f_{eff}, r^c_{eff}, v^c_{eff}\right)$ and refractive index $\left(m^f_{i,0}, b^f_r, m^f_{i,0}, b^f_i, m^c_{r,0}, b^c_r, m^c_{i,0}, b^c_i\right)$ for fine/coarse mode as well as the surface reflectance have no change in those adjacent days. With these assumptions, the varying V_{total} and fmf_V (or equivalent to AOD and fine-mode fraction of AOD) for each satellite observation, together with constant weighting coefficients **w** during the multi-observations, can be retrieved. In other words, in the retrieval, we assume no change of surface reflectance and aerosol optical parameters for each mode of aerosols in multiple days, but allow the change of total aerosol amount V_{total} and its fraction of fine aerosols fmf_V. Thus, while the PC's weighting coefficients are assumed as constant during the retrieval of multiple observations, a moving time-window (say every 5 days) can be implemented in the actual retrieval algorithm, thereby allowing that the weight coefficients to gradually change with time to reflect the surface change with time. A similar example is shown in Wang et al. [48] in which a moving time-window of 20 days is used to derive VIS-NIR surface reflectance ratio for polar-orbiting satellite, MODIS. For Geostationary satellite, we expect that this time window can be shortened to less than one week.

Same as for the simulation of those cases for analyzing individual observation, 50 vegetated spectra and 10 different AOD from 0.05 to 1.0 (i.e., a total of 500 cases) are considered to simulate the multiple observations. Therefore, the results for 3 multi-observations means that the analysis is conducted for $C^3_{10} = 120$ combinations of 3 AOD values out of 10 AOD values; only the mean DFS and standard deviation from these 120 cases are shown. In addition to the analysis for 3 multi-observation cases, 7 multi-observation cases are also shown.

Fig. 10 presents the mean DFS and standard deviation of retrieving $\{r_{eff}, V_{total}, fmf_V\}$ from three and seven multi-observation cases. As long as $\tau_a \geq 0.1$, at least 2 aerosol parameters (V_{total}, r_{eff})

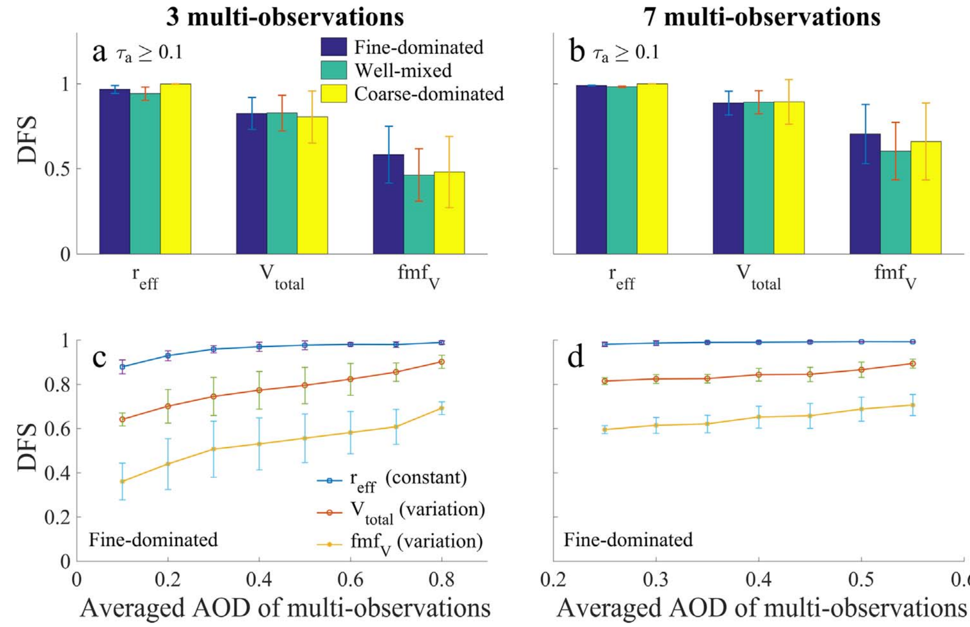

Fig. 10. Mean and standard deviation of DFS for the retrieval of aerosol parameters by the common bands of multi-observations cases in the range of 400–700 nm when $\tau_a \geq 0.1$. The dominated-mode r_{eff} and four PCs' weighting coefficients are assumed as constant in the multi-observations, while V_{total} and fmf_V vary in each observation. Left panels are for 3 adjacent multi-observations and right panels are for 7 adjacent multi-observations. Panel (a) and (c) present the averaged DFS and standard deviation for retrieval combination of $\{r_{eff}, V_{total}, fmf_V\}$; panel (c) and (d) present the mean and standard deviation of DFS as a function of AOD for multi-observations.

could be retrieved, and the more observations (e.g., from three to seven) are considered, the larger the DFS will be. For example, when 3 multi-observations are considered, fmf_V could be retrieved with V_{total} and r_{eff} only for fine-mode aerosol dominated cases; but fmf_V could be retrieved for all cases by 7 multi-observations.

Similar as Fig. 10, Fig. 11 shows the averaged DFS and standard deviation for retrieving $\{r_{eff}, V_{total}, m_{r,0}, b_r\}$. At least, three aerosol parameters could be retrieved together with four weighting coefficients. It is striking to find that the refractive index ($m_{r,0}$, b_r, that is assumed to be constant during the retrieval period) could also be retrieved together with r_{eff} and varied V_{total} (that are also constant in the retrieval period) in multiple observations for the fine-dominated aerosol model. For coarse-dominated aerosol model, the parameter b_r is still difficult to be retrieved due to the inadequate information content. For the results of four weighting coefficients, the DFS values are all larger than 0.95 in most cases (figure not shown).

In the analysis above, we have assumed that the aerosol properties for the bi-modes and the surface reflectance are constant during the multiple observations, and only the V_{total} and fmf_V vary in each observing time. While this assumption is reasonable in most conditions, long-range transport of aerosols can make this assumption invalid. For example, the smoke or dust particles may occur in one day during multiple observations. How many aerosol parameters could be retrieved in this case? To answer this question, Fig. 12 show some cases of mean DFS to retrieve 2–3 aerosol parameters with the assumption that the surface reflectance has been obtained from previous days where AOD change follows

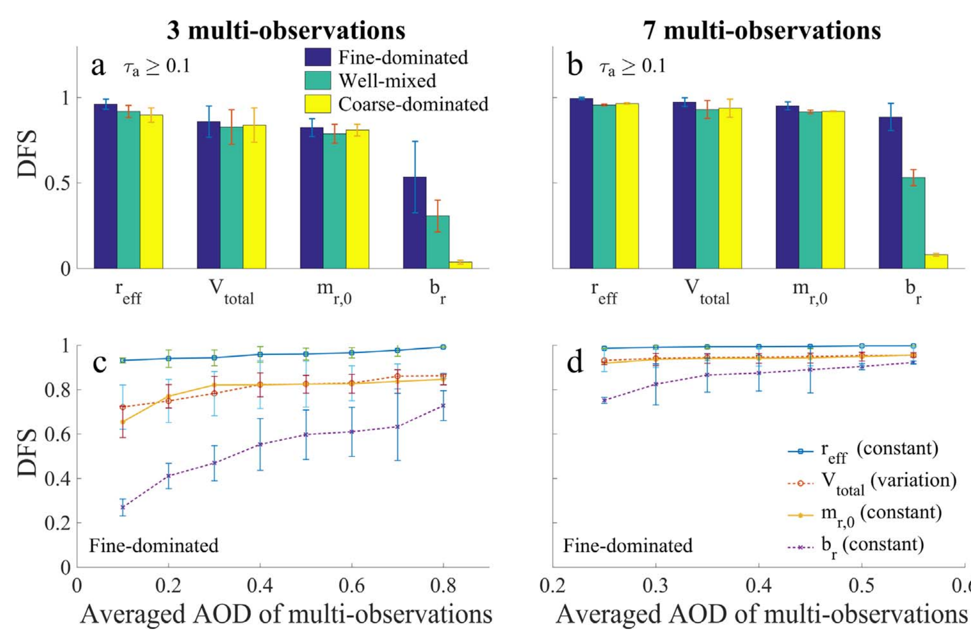

Fig. 11. Similar as Fig. 10, but for the retrieval combination of $\{r_{eff}, V_{total}, m_{r,0}, b_r\}$. Varied V_{total} and constant dominated-mode $\{r_{eff}, m_{r,0}, b_r\}$ are assumed for the retrieval.

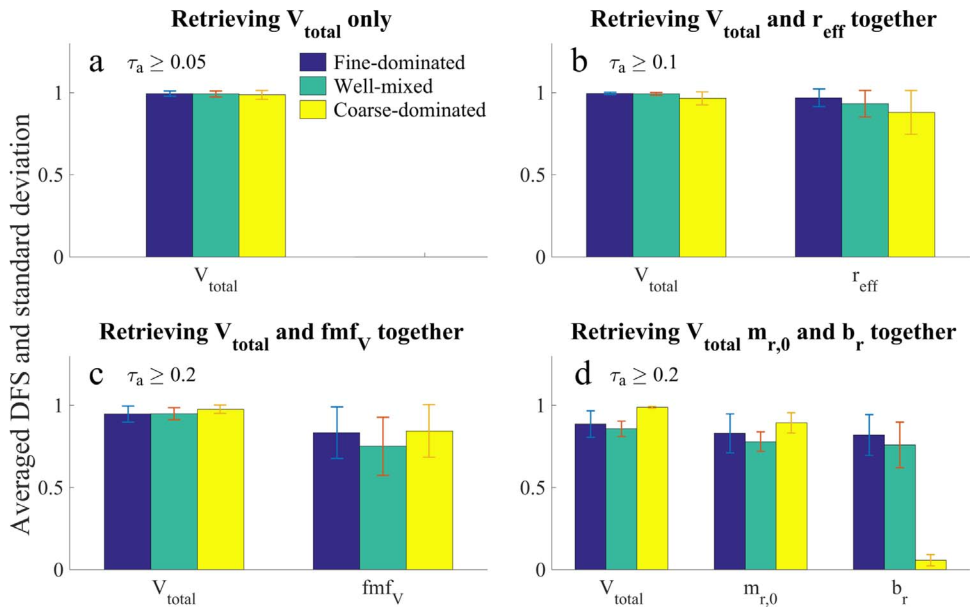

Fig. 12. Similar as Fig. 7, but for the retrieval of aerosol parameters given the surface reflectance is pre-determined.

climatology and no smoke or dust particles are detected. Compared with information content results shown in Fig. 7, the DFS in this figure are significantly improved, for the reason that the surface reflectance has been known and does not need to be retrieved. In this condition, as long as $\tau_a \geq 0.05$, V_{total} could be easily retrieved, with the DFS larger than 0.99 for all of the 3 aerosol models; and if $\tau_a \geq 0.1$, the combination of $\{V_{total}, r_{eff}\}$ could be further retrieved. When $\tau_a \geq 0.2$, we can select to retrieve the combination of $\{V_{total}, fmf_V\}$ or $\{V_{total}, m_{r,0}, b_r\}$ in most cases, except for the retrieval of b_r with coarse-dominated aerosol model. Therefore, if the surface reflectance is determined prior to aerosol retrieval, the information content can satisfy the retrieval of 1–3 aerosol parameters depend on the AOD value and the selection of state vector.

5. Conclusion and discussion

As the second part of a series of studies for retrieving aerosol properties from the hyperspectral radiances measured by new the instrument GEO-TASO and future geostationary satellite TEMPO, we conduct information content analysis for aerosol parameters and principal components of surface spectra. Our findings can be summarized into five parts, as follows.

(a) The PCs of hyperspectral surface spectra in the window channels in the spectral range 400–2400 nm and its subset (such as 400–700 nm) can be derived from TOA hyperspectral reflectance after the Rayleigh correction in low AOD conditions ($\tau_a \leq 0.2$), no matter what kind of the land surface type is. When these PCs derived from TOA spectra are used to reconstruct the surface reflectance spectra, the averaged relative error of spectral reconstruction is about 1% in comparison with the results reconstructed with 'true' surface PCs.

(b) The information content for aerosol depends on surface type, observation geometries, wavelength bands, aerosol model and the value of AOD. Among five typical surface types, the maximum values of DFS for aerosols are over green vegetation, and the minimum values of DFS are over the urban bright surface (mainly concrete). The dependence of DFS value with respect to observation geometry overall is smaller than 0.1 for each retrieval parameter.

(c) Common bands exist for hyperspectral measurements to retrieve aerosols and surface reflectance. In the visible spectrum, it is shown that ~50 common bands can be used to obtain 90% total information content. With those common bands, weighting coefficients for only 4 PCs are needed to characterize surface reflectance, thereby improving the computing efficiency for aerosol retrieval algorithm.

(d) Based on the common bands in the spectral range 400–700 nm, DFS analysis for individual observation over various surface types and AOD values have been investigated. For the vegetated surface type, when AOD $\tau_a \geq 0.2$, total aerosol volume V_{total} could be retrieved with 4 PC's weighting coefficients, and if $\tau_a \geq 0.5$, effective radius r_{eff} could be further retrieved. However, fine-mode fraction fmf_V can only be retrieved when $\tau_a \geq 0.5$ and is dominated by fine-mode aerosols.

(e) Retrievals respectively by using simultaneously three and seven observations are considered over vegetated surface. With multiple observations, 2–4 aerosol parameters can be retrieved together with 4 PC's weighing coefficients. As long as the AOD $\tau_a \geq 0.1$, at least 2 aerosol parameters (V_{total}, r_{eff}) could be retrieved together. Using seven observations can retrieve $\{r_{eff}, V_{total}, fmf_V\}$ or $\{r_{eff}, V_{total}, m_{r,0}, b_r\}$.

The findings of this study have important implication to the development of aerosol retrieval algorithm for TEMPO. TEMPO will provide hourly observation for the same location in North America, enabling more frequent sampling of backscatter hyperspectral radiance at the top of the atmosphere. According to our study here, it is expected that the PCs of surface reflectance for each TEMPO's pixel could be approximately obtained from TOA measurements at low AOD conditions. In addition to AOD, there is no single set of aerosol parameters that should be and will be retrieved for all surface types and at aerosol conditions. We show that more aerosol parameters can be retrieved from multiple measurements at the same time during consecutive days, and these retrievable parameters also depend on the number of available observations during these consecutive days as well as aerosol types and AOD. Hence, this study suggests that a self-adjustable retrieval algorithm is needed for TEMPO, which will be the focus of our next study with real observations from GEO-TASO.

Acknowledgement

Funding for this study was provided by the NASA Earth Science Division as part of NASA's GEO-CAPE and TEMPO mission study (NNX14AH10G) as well as Office of Naval Research (ONR's) Multidisciplinary University Research Initiatives (MURI) Program under the award N00014-16-1-2040. J. Wang is grateful to Jassim (Jay) A. Al-Saadi and GEO-TASO team for their encouragement, and thanks the GEO-CAPE aerosol working group and science working group for their constructive suggestions and fruitful discussions. The Holland Computing Center of University of Nebraska – Lincoln and NASA High End Computing program are acknowledged for their help in computing.

References

[1] King MD, Kaufman YJ, Tanré D, Nakajima T. Remote Sensing of tropospheric aerosols from space: past, present and future. Bull Am Meteorol Soc 1999;80:2229–2259.
[2] Kokhanovsky AA, Breon FM, Cacciari A, Carboni E, Diner D, Di Nicolantonio W, et al. Aerosol remote sensing over land: a comparison of satellite retrievals using different algorithms and instruments. Atmos Res 2007;85:372–394.
[3] Litvinov P, Hasekamp O, Cairns B. Models for surface reflection of radiance and polarized radiance: comparison with airborne multi-angle photopolarimetric measurements and implications for modeling top-of-atmosphere measurements. Remote Sens Environ 2011;115:781–792.
[4] Levy RC, Remer LA, Mattoo S, Vermote EF, Kaufman YJ. Second-generation operational algorithm: retrieval of aerosol properties over land from inversion of Moderate Resolution Imaging Spectroradiometer spectral reflectance. J Geophys Res: Atmos 112, 2007.
[5] Levy RC, Remer LA, Kleidman RG, Mattoo S, Ichoku C, Kahn R, et al. Global evaluation of the Collection 5 MODIS dark-target aerosol products over land. Atmos Chem Phys 2010;10:10399–10420.
[6] Hsu NC, Si-Chee T, King MD, Herman JR. Aerosol properties over bright-reflecting source regions. IEEE T Geosci Remote 2004;42:557–569.
[7] Hsu NC, Si-Chee T, King MD, Herman JR. Deep blue retrievals of asian aerosol properties during ACE-Asia. IEEE Trans Geosci Remote 2006;44:3180–3195.
[8] Torres O, Decae R, Veefkind JP, De Leeuw G. OMI algorithm theoretical basis document volume III: clouds, aerosols, and surface UV irradiance. In: Stammes P, editor; 2002.
[9] Torres O, Tanskanen A, Veihelmann B, Ahn C, Braak R, Bhartia PK, et al. Aerosols and surface UV products from Ozone Monitoring Instrument observations: an overview. J Geophys Res 112, 2007.
[10] Di Nicolantonio W, Cacciari A, Scarpanti S, Ballista G, Morisi E, Guzzi R. SCIAMACHY TOA reflectance correction effects on aerosol optical depth retrieval. In: Proceedings of the First Atmospheric Science Conference. Frascati, Italy; 2006.
[11] von Hoyningen-Huene W, Freitag M, Burrows JB. Retrieval of aerosol optical thickness over land surfaces from top-of-atmosphere radiance. J Geophys Res: Atmos 2003;108.
[12] Santer R, Carrere V, Dubuisson P, Roger JC. Atmospheric correction over land for MERIS. Int J Remote Sens 1999;20:1819–1840.
[13] Diner DJ, Beckert JC, Reilly TH, Bruegge CJ, Conel JE, Kahn RA, et al. Multi-angle Imaging SpectroRadiometer (MISR) instrument description and experiment overview. IEEE Trans Geosci Remote 1998;36:1072–1087.
[14] Kahn RA, Gaitley BJ, Martonchik JV, Diner DJ, Crean KA, Holben B. Multiangle Imaging Spectroradiometer (MISR) global aerosol optical depth validation based on 2 years of coincident Aerosol Robotic Network (AERONET) observations. J Geophys Res: Atmos 110, 2005.
[15] Martonchik JV, Kahn RA, Diner DJ. Retrieval of aerosol properties over land using MISR observations. In: Kokhanovsky AA, de Leeuw G, editors. Satellite aerosol remote sensing over land. Chichester, UK: Springer; 2009. p. 267–292.
[16] Chen W-T, Kahn RA, Nelson D, Yau K, Seinfeld JH. Sensitivity of multiangle imaging to the optical and microphysical properties of biomass burning aerosols. J Geophys Res 113, 2008.
[17] Thomas GE, Carboni E, Sayer AM, Poulsen CA, Siddans R, Grainger RG. Oxford-RAL Aerosol and Cloud (ORAC): aerosol retrievals from satellite radiometers. In: Kokhanovsky AA, de Leeuw G, editors. Satellite aerosol remote sensing over land. Chichester, UK: Springer; 2009. p. 193–225.
[18] Sayer AM, Thomas GE, Grainger RG, Carboni E, Poulsen C, Siddans R. Use of MODIS-derived surface reflectance data in the ORAC-AATSR aerosol retrieval algorithm: impact of differences between sensor spectral response functions. Remote Sens Environ 2012;116:177–188.
[19] Deuzé JL, Bréon FM, Devaux C, Goloub P, Herman M, Lafrance B, et al. Remote sensing of aerosols over land surfaces from POLDER-ADEOS-1 polarized measurements. J Geophys Res: Atmos 2001;106:4913–4926.
[20] Herman M. Aerosol remote sensing from POLDER/ADEOS over the ocean: improved retrieval using a nonspherical particle model. J Geophys Res 110, 2005.
[21] Zhang Y, Li Z, Qie L, Zhang Y, Liu Z, Chen X, et al. Retrieval of aerosol fine-mode fraction from intensity and polarization measurements by PARASOL over East Asia. Remote Sens 8, 2016.
[22] Aumann HH, Chahine MT, Gautier C, Goldberg MD, Kalnay E, McMillin LM, et al. AIRS/AMSU/HSB on the Aqua mission: design, science objectives, data products, and processing systems. IEEE Trans Geosci Remote 2003;41:253–264.
[23] De Souza-Machado SG, Strow LL, Hannon SE, Motteler HE. Infrared dust spectral signatures from AIRS. Geophys Res Lett 33, 2006.
[24] De Souza-Machado SG, Strow LL, Imbiriba B, McCann K, Hoff RM, Hannon SE, et al. Infrared retrievals of dust using AIRS: comparisons of optical depths and heights derived for a North African dust storm to other collocated EOS A-Train and surface observations. J Geophys Res 115, 2010.
[25] Wang J, Christopher SA. Mesoscale modeling of Central American smoke transport to the United States: 2. Smoke radiative impact on regional surface energy budget and boundary layer evolution. J Geophys Res 111, 2006.
[26] Leitch JW, Delker T, Good W, Ruppert L, Murcray F, Chance K., et al. The GeoTASO airborne spectrometer project. In: Proceedings SPIE 9218, Earth Observing Systems XIX. p. 92181H1-92189H; 2014.
[27] Zoogman P, Liu X, Suleiman RM, Pennington WF, Flittner DE, Al-Saadi JA, et al. Tropospheric emissions: monitoring of pollution (TEMPO). J Quant Spectrosc Radiat 186, 2017, 17-39.
[28] Nowlan CR, Liu X, Leitch JW, Chance K, González Abad G, Liu C, et al. Nitrogen dioxide observations from the Geostationary Trace gas and Aerosol Sensor Optimization (GeoTASO) airborne instrument: retrieval algorithm and measurements during DISCOVER-AQ Texas 2013. Atmos Meas Tech 2016;9:2647–2668.
[29] Wang J, Xu X, Ding S, Zeng J, Spurr R, Liu X, et al. A numerical testbed for remote sensing of aerosols, and its demonstration for evaluating retrieval synergy from a geostationary satellite constellation of GEO-CAPE and GOES-R. J Quant Spectrosc Radiat 2014;146:510–528.
[30] Lee CM, Cable ML, Hook SJ, Green RO, Ustin SL, Mandl DJ, et al. An introduction to the NASA Hyperspectral InfraRed Imager (HyspIRI) mission and preparatory activities. Remote Sens Environ 2015;167:6–19.
[31] Thompson DR, Gao B-C, Green RO, Roberts DA, Dennison PE, Lundeen SR. Atmospheric correction for global mapping spectroscopy: ATREM advances for the HyspIRI preparatory campaign. Remote Sens Environ 2015;167:64–77.
[32] Hou W, Wang J, Xu X, Reid JS, Han D. An algorithm for hyperspectral remote sensing of aerosols: 1. Development of theoretical framework. J Quant Spectrosc Ra 2016;178:400–415.
[33] Rodgers CD. Inverse methods for atmospheric sounding: theory and practice. Singapore: World Scientific; 2000.
[34] Xu X, Wang J. Retrieval of aerosol microphysical properties from AERONET photopolarimetric measurements: 1. Information content analysis. J Geophys Res: Atmos 2015;120:7059–7078.
[35] Xu X, Wang J, Zeng J, Spurr R, Liu X, Dubovik O, et al. Retrieval of aerosol microphysical properties from AERONET photopolarimetric measurements: 2. A new research algorithm and case demonstration. J Geophys Res: Atmos 2015;120:7079–7098.
[36] Dubovik O, King MD. A flexible inversion algorithm for retrieval of aerosol optical properties from Sun and sky radiance measurements. J Geophys Res: Atmos 2000;105:20673–20696.
[37] Hess M, Koepke P, Schult I. Optical properties of aerosols and clouds: the software package OPAC. Bull Am Meteorol Soc 1998;79:831–844.
[38] Patterson EM, Gillette DA, Stockton BH. Complex index of refraction between 300 and 700 nm for Saharan aerosols. J Geophys Res 1977;82:3153–3160.
[39] Wagner R, Ajtai T, Kandler K, Lieke K, Linke C, Müller T, et al. Complex refractive indices of Saharan dust samples at visible and near UV wavelengths: a laboratory study. Atmos Chem Phys 2012;12:2491–2512.
[40] Clark RN, Swayze GA, Wise R, Livo E, Hoefen T, Kokaly R, et al. USGS digital spectral library splib06a: u.s. Geological Survey. Digit Data Ser 2007;231. ⟨http://speclab.cr.usgs.gov/spectral.lib06⟩.
[41] Baldridge AM, Hook SJ, Grove CI, Rivera G. The ASTER spectral library version 2.0. Remote Sens Environ 2009;113:711–715.
[42] Torres O, Ahn C, Chen Z. Improvements to the OMI near-UV aerosol algorithm using A-train CALIOP and AIRS observations. Atmos Meas Tech 2013;6:3257–3270.
[43] Wang J, Christopher SA, Reid JS, Maring H, Savoie D, Holben BN, et al. GOES 8 retrieval of dust aerosol optical thickness over the Atlantic Ocean during PRIDE. J Geophys Res: Atmos 108, 2003.
[44] Wang J, Christopher SA, Brechtel F, Kim J, Schmid B, Redemann J, et al. Geostationary satellite retrievals of aerosol optical thickness during ACE-Asia. J Geophys Res: Atmos 108, 2003.
[45] Zhang J, Christopher SA, Holben BN. Intercomparison of smoke aerosol optical thickness derived from GOES 8 imager and ground-based Sun photometers. J Geophys Res: Atmos 2001;106:7387–7397.
[46] Christopher SA, Zhang J, Holben BN, Yang SK. GOES-8 and NOAA-14 AVHRR retrieval of smoke aerosol optical thickness during SCAR-B. Int J Remote Sens 2002;23:4931–4944.
[47] Knapp KR, Frouin R, Kondragunta S, Prados A. Toward aerosol optical depth retrievals over land from GOES visible radiances: determining surface reflectance. Int J Remote Sens 2005;26:4097–4116.
[48] Wang J, Xu X, Spurr R, Wang Y, Drury E. Improved algorithm for MODIS satellite retrievals of aerosol optical thickness over land in dusty atmosphere: implications for air quality monitoring in China. Remote Sens Environ 2010;114:2575–2583.

[49] Smith RB. Introduction to hyperspectral imaging. MicroImages, Inc.; 2012.
[50] Wang J, Xu X, Henze DK, Zeng J, Ji Q, Tsay S.-C, Top-down estimate of dust emissions through integration of MODIS and MISR aerosol retrievals with the GEOS-Chem adjoint model Geophys Res Lett 39:2012.
[51] Kaufman YJ, Tanre D, Boucher O. A satellite view of aerosols in the climate system. Nature 2002;419:215–223.
[52] Remer LA, Tanré D, Kaufman YJ, Levy R, Mattoo S. Algorithm for remote sensing of tropospheric aerosol from MODIS: collection 5, Product ID: MOD04/MYD04. NASA Goddard Space Flight Center; 2006.
[53] Bodhaine BA, Wood NB, Dutton EG, Slusser JR. On Rayleigh optical depth calculations. J Atmos Ocean Tech 1999;16:1854–1861.
[54] Tomasi C, Vitale V, Petkov B, Lupi A, Cacciari A. Improved algorithm for calculations of Rayleigh-scattering optical depth in standard atmospheres. Appl Opt 2005;44:3320.
[55] Frankenberg C, Hasekamp O, O'Dell C, Sanghavi S, Butz A, Worden J. Aerosol information content analysis of multi-angle high spectral resolution measurements and its benefit for high accuracy greenhouse gas retrievals. Atmos Meas Tech 2012;5:1809–1821.
[56] Veihelmann B, Levelt PF, Stammes P, Veefkind JP. Simulation study of the aerosol information content in OMI spectral reflectance measurements. Atmos Chem Phys 2007;7:3115–3127.
[57] Tanré D, Herman M, Kaufman YJ. Information on aerosol size distribution contained in solar reflected spectral radiances. J Geophys Res: Atmos 1996;101:19043–19060.
[58] Hasekamp OP, Landgraf J. Retrieval of aerosol properties over the ocean from multispectral single-viewing-angle measurements of intensity and polarization: retrieval approach, information content, and sensitivity study. J Geophys Res 110, 2005.
[59] Holzer-Popp T, Schroedter-Homscheidt M, Breitkreuz H, Martynenko D, Klüser L. Improvements of synergetic aerosol retrieval for ENVISAT. Atmos Chem Phys 2008;8:7651–7672.
[60] Martynenko D, Holzer-Popp T, Elbern H, Schroedter-Homscheidt M. Understanding the aerosol information content in multi-spectral reflectance measurements using a synergetic retrieval algorithm. Atmos Meas Tech 2010;3:1589–1598.
[61] Li S, Qiu J, Yang X, Liu H, Wan D, Zhu Y. A novel approach to hyperspectral band selection based on spectral shape similarity analysis and fast branch and bound search. Eng Appl Artif Intel 2014;27:241–250.
[62] Yang H, Du Q, Su H, Sheng Y. An efficient method for supervised hyperspectral band selection. IEEE Geosci Remote Sens Lett 2011;8:138–142.
[63] Dubovik O, Smirnov A, Holben BN, King MD, Kaufman YJ, Eck TF, et al. Accuracy assessments of aerosol optical properties retrieved from Aerosol Robotic Network (AERONET) Sun and sky radiance measurements. J Geophys Res: Atmos 2000;105:9791–9806.
[64] Holben BN, Eck TF, Slutsker I, Tanré D, Buis JP, Setzer A, et al. AERONET—a federated instrument network and data archive for aerosol characterization. Remote Sens Environ 1998;66:1–16.
[65] Holben BN, Tanré D, Smirnov A, Eck TF, Slutsker I, Abuhassan N, et al. An emerging ground-based aerosol climatology: aerosol optical depth from AERONET. J Geophys Res: Atmos 2001;106:12067–12097.
[66] Xu X, Wang J, Henze DK, Qu W, Kopacz M. Constraints on aerosol sources using GEOS-Chem adjoint and MODIS radiances, and evaluation with multisensor (OMI, MISR) data. J Geophys Res: Atmos 2013;118:6396–6413.
[67] Hagolle O, Dedieu G, Mougenot B, Debaecker V, Duchemin B, Meygret A. Correction of aerosol effects on multi-temporal images acquired with constant viewing angles: application to Formosat-2 images. Remote Sens Environ 2008;112:1689–1701.